THE MOLECULAR SPECTRUM OF SUNSPOTS

Thesis by

John C. Webber

In Partial Fulfillment of the Requirements

For the Degree of

Doctor of Philosophy

California Institute of Technology

Pasadena, California

1970

(Submitted September 2, 1969)

To My Wife

ACKNOWLEDGEMENTS

It is a pleasure to thank Prof. Harold Zirin for suggesting this area of investigation, and for much patient guidance and encouragement.

Thanks are due also to David Lambert for helpful discussions, and to Mitsugu Makita for some clarifications.

Special mention must be given to Tom Cragg and Merwin Utter for assistance with the 150-foot tower, and for helping find the good seeing conditions needed for this project.

My thanks to Dr. Eugene Cowan for graciously extending the photographic facilities of the Cosmic Ray Lab, and to Willem for help there.

Thanks also to those crews in Astro Electronics and Booth Computing Center whose efforts make the machinery do what we want it to.

It is a pleasure to acknowledge the financial support of a NASA Traineeship, as well as a Graduate Teaching Assistantship and Graduate Research Assistantship. Part of this work was supported by NASA Grant # NGR 05002034.

ABSTRACT

The sunspot spectrum shows many molecular lines, of which some have been identified. These lines are formed farther out in the sunspot atmosphere than the atomic lines or the continuum, and are thus useful for probing the outer layers. Photographic spectrograms were obtained for three different sunspots under carefully selected seeing conditions, showing molecular absorption lines due to MgH, CaH, and TiO. Analysis led to estimates of the effective rotational temperatures of each; in the case of CaH, no definite conclusions could be drawn. Predicted rotational temperatures and observational f-values were calculated on the basis of model umbral atmospheres due to several authors. A new model was derived from the molecular lines measured here, and shown to differ widely from previous models. The usefulness of photographic spectra for this purpose is seriously questioned, and suggestions are made for new observations.

TABLE OF CONTENTS

INTRODUCTION

It has been known for a long time that the sunspot spectrum shows many lines due to molecular absorption. Some of the molecular species known to be present are seen only in the sunspot spectrum, while others are seen in the disk spectrum as well, and are strengthened or weakened in the spot (Moore et al., 1966). From time to time, many authors have claimed to find molecular band heads of various improbable molecules, but the claims are extremely dubious (see, for example, Babcock, 1945). At high dispersion, the sunspot spectrum is exceedingly complex; it is doubtful that the true continuum is often reached except in the red and the infrared, where fewer weak lines are present. However, for several molecules, individual absorption lines can be picked out; and only if a rotational analysis and comparison with laboratory data can be made is it possible to prove the existence of a given molecule.

The structure of the sunspot atmosphere is highly uncertain, due primarily to problems involving the effects of magnetic fields on theory (Chitre and Shaviv, 1967) and of scattered light on the observations. Models computed by various authors differ widely, according to the computational procedure and type of data employed. To date, the primary observational

material involved in model construction has been the atomic lines and continuum radiation, both of which are highly susceptible to contamination by small amounts of scattered light from the disk.

Makita (1968) has made a short investigation of the compatibility of various models with the TiO spectrum near λ5250, but otherwise no author has incorporated molecular data in a comprehensive manner. In particular, the very outermost layers of the umbral atmosphere are highly uncertain, due to the small contribution to the atomic spectrum and continuum radiation from the layers with optical depth less than 0.1.

Figure 2 shows some results of calculations described later. Contribution functions are shown for TiO, CaH, and MgH, and for weak Fe I lines of excitation potentials 0.0 and 4.5 eV, for the principal model of Zwaan (1965).

It may be seen that MgH corresponds approximately to weak Fe I lines with excitation potential 4 eV, and that CaH corresponds roughly to weak Fe I lines with excitation potential 0 eV. These two molecules must therefore tell us approximately the same information as the atomic spectrum; this provides a sort of check of reliability of the molecular data. However, the TiO is formed much farther out in the atmosphere. Not

shown here is the contribution function for the molecule ZrO; it corresponds to a case about half-way between TiO and CaH.

Since the contribution function for TiO has an appreciable magnitude at very small optical depths, it is uniquely qualified to yield information about those layers.

The use of the molecular spectrum, although highly desirable from a theoretical standpoint, is difficult to put into practice for several reasons. First is the difficulty in obtaining spectra suitable for rotational analysis. The contrast between umbra and surrounding penumbra and disk is very great in visible wavelengths, making scattered light a serious problem for both spectroscopy and photometry. It is difficult to estimate even roughly the amount of light scattered into the spot spectrum in the atmosphere of the Earth and the equipment.

Fortunately, for obtaining rotational temperatures the total amount of scattered light is irrelevant, as long as it remains constant while the spectrograms are being taken. In particular, there must be no systematic change in the amount of scattered light as a function of rotational quantum number J. The f-values calculated from comparison of observation

with calculation will be affected by scattered light, but this is a relatively minor consideration, since precise f-values from laboratory work are lacking.

Since the dispersions employed for satisfactory resolution of these weak rotational lines are very large, and hundreds of Angstroms of spectrum must be covered to obtain a suitable range of J, the following are necessary:

(a) the best seeing--stability is most important;

(b) a large, stable sunspot must be present;

(c) the use of film is desirable, so that large numbers of plateholders need not be loaded and handled during hurried exposures.

A second important difficulty, even with the best observational material, involves the uncertainty in continuum level and the possibility of undetected blends. To insure accuracy, a special measuring procedure must be employed, which will be discussed later.

I. OBSERVATIONS

I made several attempts to record the spectra of all the molecules found in sunspots, using the same spot, and under the same seeing conditions. This proved impossible; however, overlapping regions were obtained for two cases.

All spectra were taken with the 150-foot tower and 75-foot pit spectrograph at Mt. Wilson. Fifth-order spectrograms were taken between λλ5000--5500 at reciprocal dispersion of 10.8 to 12.9 mm/A on Plus-X Pan film, with exposure times from 20 to 30 seconds. Fourth-order spectrograms were taken between λλ6200--7000 on Aerecon Plus-X film, with exposure times from 5 to 10 seconds. In all cases, a mask was used to permit exclusion of scattered light in the instrument; during the last 15% of each exposure, the slit was lengthened to record the disk spectrum for purposes of identification and comparison.

Photographs in white light were taken of each spot on 35mm film at intervals during taking the spectrograms, to provide definite information on the possible deterioration of seeing conditions and the amount of scattered light. Exposures were 1/10 second through an NG1 filter on Panatomic-X; since the purpose was essentially photometric, I made no effort to use

a wide field or eliminate every last dust particle on film and filter. Subsequent evaluation of the white-light photographs led to discarding spectrograms taken when seeing had deteriorated significantly, thus preserving the criterion that there must be no change in the amount of scattered light over a wide range in wavelength.

All spectrograms were developed in D-19 for 12 to 15 minutes and traced on the Cal Tech microphotometer.

Two of the sunspots chosen were old, round spots which had been stable for several days and showed no significant internal structure other than granulation in the umbra. One large spot (of 10/28/68) was in an old group, which was highly active at the time, but nonetheless remained stable during observation. Since all the umbras were symmetrical (aside from the small effect of viewing angle), I made no effort to orient the spectrograph slit in any particular direction. In each case, the slit length was about 80% of the width of the umbra, and was centrally positioned. All spots were near meridian passage at the time of observation (0.25 to 0.5 R from the center of the disk); usable observations are listed in Table 1. The umbral area in solar hemispheres and the approximate amount of scattered light are listed.

Table 1

Date	Area, s.h.	% Scat.	λλ	Molecules
9/27/68	33×10^{-6}	10-15	6750--7000	CaH A
10/28/68	100	10	5000--5500	MgH, TiO
1/ 7/69	42	50	5000--5400	TiO
		20-30	6240--6560	CaH B

Spectrograms taken in the red are less susceptible to contamination by scattered light than in the green, due to the decreased contrast between umbra and disk. There is, however, greater interference from atmospheric lines; accordingly, spectrograms in the red were taken at higher solar altitudes when possible.

Intensity calibration was by means of a deposited-metal step-filter placed across the length of the slit. This method is subject to some uncertainty, but the error is not important in this case.

II. HISTORY OF SPOTS OBSERVED

The following descriptions are derived from the data compiled by ESSA (1968, 1969) and from observations made during the course of this investigation.

The spot of 9/27/68 first appeared at the limb of the sun on 8/28/68, near the position of an old group. At the time of observation, it was a single round umbra associated with a small amount of pore structure, aged 30 to 45 days. It was located at about 13° N, 30° E, with $\cos \theta = 0.88$. Two days after observation, it began to break up.

The spot of 10/28/68 appeared as a newly developing group on 9/2/68, on the visible disk. After showing some activity, it turned into a single isolated spot around 10/4/68. Reappearance at the limb on 10/22/68 showed it to be enormously active again. At the time of observation, it was a large and complex group, with a single large preceding umbra, aged 56 days. It was located at about 14° S, 0° longitude, with $\cos \theta = 0.95$. After observation, the size and complexity slowly dwindled until final disappearance on 12/1/68.

The spot of 1/7/69 first appeared as a newly developing group on 12/15/68, on the visible disk. After some initial activity, it settled down to being

a single round spot with a few occasional pores associated. At the time of observation, it was a single umbra, aged 23 days, with some nearby pore structure. It was located at about 25° N, 10° E, with cos θ = 0.87. After observation, it remained rather stable and quiescent until disappearance on 2/11/69.

It may be seen from the foregoing descriptions that the spots of 9/27/68 and 1/7/69 had similar sizes, ages, and histories, while that of 10/28/68 is quite different. Nevertheless, except for total amount of scattered light, the spectral region λλ5000--5400 recorded both 10/28/68 and 1/7/69 shows nearly identical results for rotational temperature for TiO. This is in accord with the idea that a sunspot umbra has essentially the same structure, regardless of size, shape, or history. No conclusions about absolute line strengths are possible on the basis of this data, however.

III. ANALYSIS

For a gas composed of molecules all at the same temperature, the strengths of the rotational lines are given by Herzberg (1950):

$$\log(W_J/S_J) = C - \frac{0.625\ F_V(J)}{T} \qquad (1)$$

where

W_J = equivalent width of line J

S_J = theoretical line strength

$F_V(J)$ = rotational term values

T = temperature

C = nearly a constant

It is therefore possible to obtain what should be called the "effective rotational temperature" $T_{eff,rot} = T_{er}$ by plotting $\log(W_J/S_J)$ against $F_V(J) = B_V J(J+1) - D_V J^2(J+1)^2$ and measuring the slope. This has been applied to the solar disk and sunspot spectrum by several authors (Laborde, 1961; Makita, 1968; Schadee, 1964).

In practice, several difficulties arise. First is the difficulty in measuring W_J in a spectrum as complex as that of a sunspot. A reasonable method is employed by Makita (1968). Here, a minimum value for W_J is obtained by assuming that the local continuum is the true continuum; a maximum value is obtained

by assuming the true continuum is at the level of the highest continuum present nearby (thus enters subjective judgment). If enough lines can be measured this way, it can be expected that at least a few measurements will be accurate. One then draws a straight line through the maximum envelope of the minimum measurements, and a straight line through the minimum envelope of the maximum measurements. Ideally, these lines would coincide and have the same slope. Also, for any lines having the same local and overall continuum, the measurements should lie close to both envelopes. In practice, some overlap is unavoidable.

This method of treating the W_J's is susceptible to two main sources of error: first, the minimum W_J's are easily increased by blends with lines which are not seen in the disk spectrum; second, the maximum W_J's may be decreased because the true continuum is not reached anywhere near the line. It may therefore be expected that a few lines will lie outside tne envelopes drawn. Only subjective judgment or additional data can eliminate these bad points. Despite these shortcomings, Makita's method has been adopted here as being probably more reliable than any other.

A second difficulty in applying Equation (1) is that the theoretical S_J values may be difficult to

obtain with sufficient accuracy, particularly for low J values. Formulas for S_J are given in many places for various types of transitions (Herzberg, 1950; Mulliken, 1931; Schadee, 1964). It will be shown here that the relative strengths of P, Q, and R branches for CaH are clearly at variance with observation, and very bad for the lowest J values. The rotational temperatures obtained for this molecule are thus highly doubtful.

A third difficulty in applying Equation (1) is that the quantity C is nearly constant only for small ranges of wavelength and temperature. Therefore, much caution must be used when relating the measured T_{er} to a theoretical calculation based on some model atmosphere.

It should also be noted that the slope obtained from a plot of $\log(W_J/S_J)$ against $F_v(J)$ is proportional to 1/T. Therefore, when averaging several T_{er}'s obtained from different data, one should take a harmonic mean.

Figure 1 shows microphotometer tracings for three lines included in the list of good lines described later. The line due to CaH A(0,0) $Q_2(13)$ is typical of those for which the local and overall continuum levels appear identical. The other two examples show

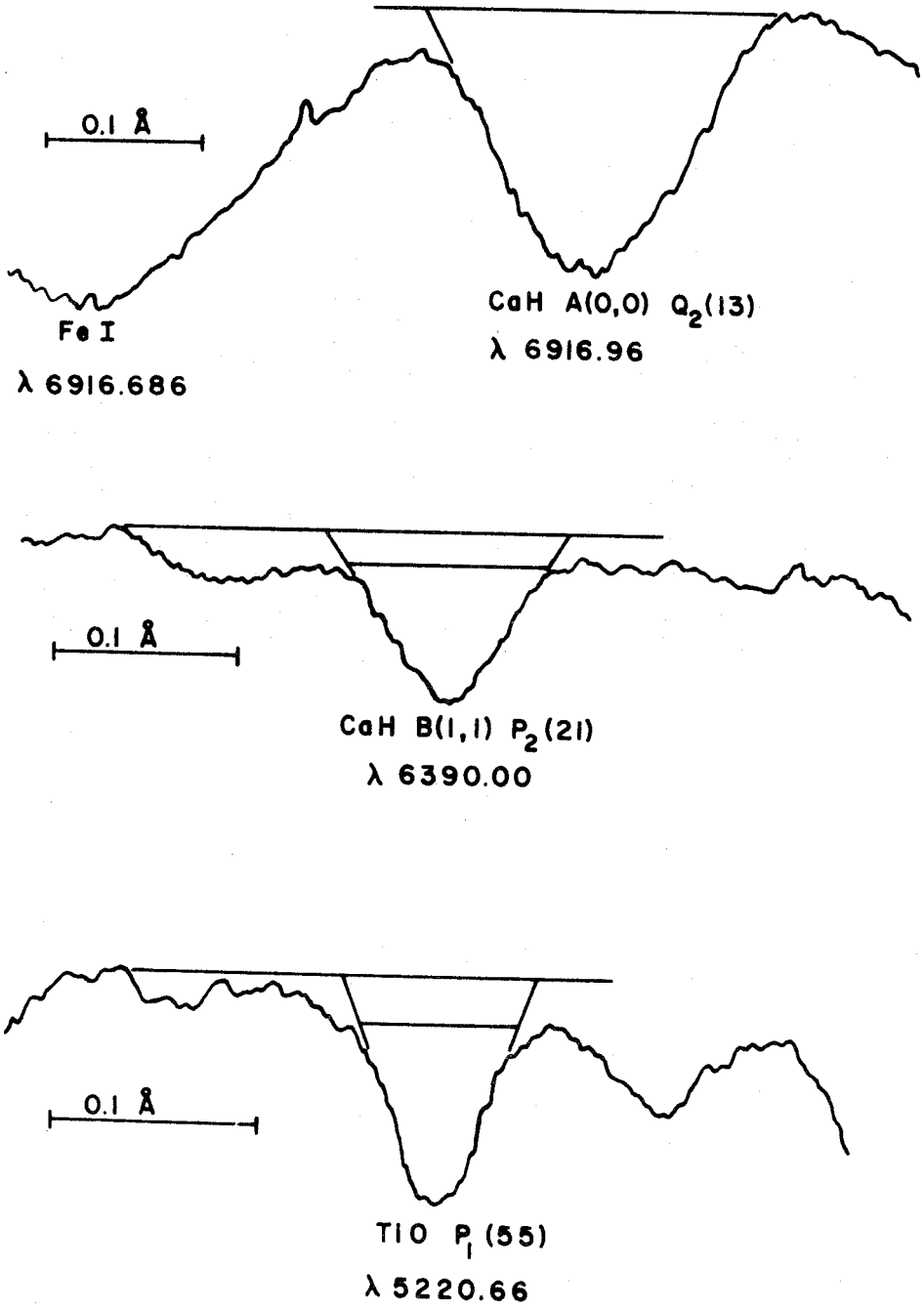

Figure 1. Typical tracings of good quality lines. Residual intensities at the centers of the molecular lines are (from top to bottom) 0.74, 0.82, 0.78.

the manner in which the continuum levels are determined and the wings of the lines extended.

Table 6 lists the lines observed for TiO and CaH, along with laboratory and measured wavelengths. Quality is indicated as follows:

1: line is definitely present, but equivalent width is difficult or impossible to measure;

2: line is imperfect but usable;

3: line is of highest quality.

All lines measured in the laboratory which are hopelessly blended with atmospheric, atomic, or other molecular lines are omitted from Table 6.

The measurements actually made in this investigation will now be discussed.

A. The Molecule TiO

A few prior measurements of TiO have been made (Hitchcock, 1965; Makita, 1968). However, Hitchcock's analysis has been shown faulty (Schadee, 1966), and Makita's covers only 34 lines in a limited wavelength range. Fortunately, in this case, the rotational quantum numbers are large and there is apparently no difficulty with the S_J. Phillips' (1969) reclassification of this α system as a $^3\Delta$ -- $^3\Delta$ transition does not affect the S_J appreciably for these high

quantum numbers. However, it should be noted that a change of J by one unit would change T_{er} by about 80° K. Such a systematic shift would be more important than slight errors in the measurements for W_J.

TiO lines in the α band from $\lambda\lambda$5209--5300 were measured for the spots of 10/28/68 and 1/7/69; 123 and 93 lines, respectively, were measured for those two dates. Wavelengths were taken from Christy (1929). In each case, 20 lines were recorded on more than one exposure (different lines on different dates), and therefore were measured twice as a check on internal consistency and constancy of scattered light from one exposure to the next. This also constitutes a check on the positioning and (photoelectric) guiding of the spots during each exposure. The two independent measures generally agreed to within a few per cent, the principal differences being due to continuum uncertainty.

For each date, T_{er} was obtained by finding the envelopes for maximum and minimum plots for P and R branches separately and together. Results are in Table 2.

Table 2

Date	T_{er}
10/28/68	3530 ± 300° K
1/ 7/69	3430 ± 300° K

These measures agree well within the standard deviation; therefore, I shall adopt the average value 3480 ± 300° K for TiO. This value is somewhat higher than Makita's (1968) value 3030 ± 270° K. If I restrict consideration to the wavelength range which Makita had available, I obtain T_{er} = 3420 ± 300° K for the data of 10/28/68. This seems to indicate that the disagreement is not due solely to the regions of the spectrum employed.

The good agreement between the values obtained for the two spots observed here indicates there was little difference between the structures of their upper atmospheres, although they differed in umbral area by a factor of 2.5. A comparison of the absolute line strengths is impossible here, because of the greater amount of scattered light on 1/7/69.

A list of the 26 best TiO lines measured is presented in Table 7. Equivalent widths (all are in mA) in parentheses indicate lines of slightly lower quality. In those cases where only one equivalent width is

listed, the overall and local continuum levels appeared to be identical. This does not necessarily mean that the single measurement is more reliable.

Using these 26 lines only, rotational temperatures were 3660 and 3630° K for the spots of 10/28/68 and 1/7/69, respectively, with about the same error limits as for the whole set of data.

B. The Molecule MgH

A plot of $\log(W_J/S_J)$ against $F_v(J)$ has been made by Laborde (1961) for MgH in the disk and spot spectrum, and by Schadee (1964) in the disk only. I am unable to reproduce Laborde's measurements, since many of his lines seem to be badly blended with unidentified sunspot lines on my spectrograms. Laborde's final plot is of only a few lines from each branch, which scatter almost imperceptibly around a straight line, in sharp contrast to the large scatter found here and (for TiO) by Makita.

For the spot of 10/28/68, 80 lines between λλ5021--5209 were measured; there were 13 repeated measurements. Wavelengths were taken from Moore et al. (1966) and from Watson and Rudnick (1927). The larger amount of scattered light on 1/7/69 would have introduced serious problems for MgH, since its spectrum

is also seen in the disk, at a drastically different T_{er}. Therefore, the MgH lines were not measured for the spot of 1/7/69.

In the accompanying figures (see APPENDIX), it may be seen that $\log(W_J/S_J)$ for the Q branch appears to lie slightly below the P and R branches for low J values. This may be a real effect (which would indicate an inaccurate formula for the S_J), or merely observational accident. Fortunately for these purposes, the apparent error has little or no effect on the results, which are that $T_{er} = 3930 \pm 400°$ K for MgH. This value is not very different from the results of Laborde, namely $T_{er} = 3730 \pm 300°$ K.

It is difficult to find good, sharp MgH lines in the sunspot spectrum, due to the presence of many blends and strong atomic lines in the range λλ5000--5200. The nine best are listed in Table 7. The range of $F_v(J)$ is quite large, although nine lines are barely enough to determine anything. These few lines imply $T_{er} = 3970 \pm 400°$ K for MgH, which is little different from the value previously determined.

C. The Molecule CaH

The interpretation of the CaH spectra is more difficult than for TiO or MgH. The two lowest-lying

electronic transitions are A $(^2\Pi)$--X $(^2\Sigma)$ and B $(^2\Sigma)$--X $(^2\Sigma)$. In each case, both (0,0) and (1,1) bands were observed; these were analyzed separately. Wavelengths were taken from Hulthén (1927).

For A(0,0), it is clear from the plots that the values for $\log(W_J/S_J)$ are much too high for the lowest quantum numbers. This effect has been observed in laboratory absorption spectra by Liberale and Weniger (1969), although they failed to mention it explicitly. Also, for the highest J-values, the Q branch falls noticeably below the P and R branches, as for MgH. However, for the highest J-values, all seem to converge. This leads to discrepancies in the rotational temperatures obtained from individual branches, and correspondingly higher error. Taking the data at face value, I obtain $T_{er} = 3850 \pm 550°$ K for CaH A(0,0).

For the A(1,1) bands, as for A(0,0), the values of $\log(W_J/S_J)$ for low J are too high; furthermore, the Q branch lies below the P and R branches for all J. Again taking the data at face value, I obtain $T_{er} = 4660 \pm 580°$ K for CaH A(1,1). It is to be expected that T_{er} for the (1,1) band will be greater than for the (0,0) band, since the higher vibrational level will be more highly populated at larger T in

the umbral atmosphere, and will therefore weight the higher rotational levels preferentially. However, this observed difference of 810° K is much larger than calculations show possible. It is evident that a revision of these results awaits laboratory determination of S_J values.

The same situation is found in the B bands, which arise from the same ground level and should therefore yield the same rotational temperature as the A bands. In B(0,0) and (1,1), the R branch lies above the P branch for the very lowest J values, then falls rapidly to lie below it for intermediate and higher values. Taking the face value of the data again, I obtain T_{er} = 4860 ± 400° K for B(0,0) and T_{er} = 3910 ± 500° K for B(1,1). Here, the temperatures are higher for the (0,0) than for the (1,1) bands, just opposite to the situation for the A bands. I must conclude that an understanding of the CaH spectrum in sunspots awaits detailed analysis of the intensity anomalies as seen in the laboratory.

A list of the best CaH lines measured is provided in Table 7. The comments about the entries for TiO apply here, also.

When only the best lines for CaH are considered, the situation with respect to the A bands improves,

as far as rotational temperatures are concerned. For A(0,0), T_{er} = 3520 ± 300° K, and for A(1,1), T_{er} = 3350 ± 400° K. Calculations show that these bands should agree within about 50° K; therefore, I shall average these values and adopt T_{er} = 3450 ± 300° K for CaH.

Even considering only the best lines, the B bands remain an enigma. The clear disagreement between P and R branches, coupled with the too-large W_J measures for P branch lines of large J, suggests laboratory misidentification. The structure of the B bands should be reinvestigated from scratch.

D. The Molecule ZrO

The rotational lines of ZrO have long been accepted as present in the sunspot spectrum (Moore et al., 1966). I attempted to identify and measure enough lines of ZrO in the region λλ6470--6490 to obtain a rotational temperature and f-value estimate. The lines present in the spectrum were compared with the laboratory wavelengths of Lagerquist et al. (1954). Lines were present which agreed reasonably well with laboratory wavelengths, but which formed no particular pattern of intensity as a function of branch and rotational quantum number. There were also several

unaccountable gaps in the sequences of identified lines, which is an unallowable situation.

Calculations described later show that the number abundance of ZrO is from 0.04 to 0.01 times that of TiO for the model umbral atmospheres considered. In order to be present in detectable amounts, then, the f-value for ZrO would have to be much greater than for the very similar molecule TiO. I conclude that the presence of detectable amounts of ZrO in the sunspot spectrum is highly doubtful.

IV. THEORETICAL CALCULATIONS

The general expression for the equivalent width of a molecular line formed in an atmosphere is given by Schadee (1964):

$$W_J = \frac{\pi e^2}{m_e c^2} \lambda^2 (f_{el} f_v) \frac{S_J}{2J+1} \int_0^\infty g_\lambda(z)\ N_{nvJ}\ dz \qquad (2)$$

where

$f_{el}f_v$ = f-value for the transition, hereafter called simply f

$g_\lambda(z)$ = weight function

N_{nvJ} = number of molecules/cm^3 in electronic state n, vibrational state v, and rotational state J

z = physical altitude

In the cases considered here, essentially all the molecules are in the ground electronic state. Other formulas needed are given by Herzberg (1950):

$$\frac{N_v}{N} = \frac{\exp(-G(v)hc/kT)}{1+\sum_i \exp(-G(i)hc/kT)} = u(T) \qquad (3)$$

$$\frac{N_{nvJ}}{N_{nv}} = \frac{hcB_v}{kT}\ (2J+1)\ \exp(-0.625\ F_v(J)/T) \qquad (4)$$

where

B_v = rotational constant

$G(v)$ = vibrational term value for state v

In these calculations, the integration was performed in steps of log P_g; combining all these yields

$$\frac{W_J}{fS_J} = \frac{\pi he^2}{m_e ck} B_v \lambda^2 \int_{\log P_{min}}^{\log P_{max}} Ng_\lambda(P) \frac{u(T)}{T} \frac{dz}{d\log P_g} d\log P_g \qquad (5)$$

The overall procedure was as follows:

(a) at each level in the integration, compute the partial pressures of the relevant atomic and molecular species (see, for example, Tsuji, 1964), taking ionization into account;

(b) perform the integration through the atmosphere to obtain W_J/fS_J for appropriate values of J for each molecule considered;

(c) from these values, calculate a theoretical effective rotational temperature; by comparison with observed values for W_J/S_J, find f-values.

Values for the molecular equilibrium constants were taken from Tsuji (1964). The species considered were:

(a) atomic and ionic: H, He, O, Ca, Ca^+, Mg, Mg^+,

Ti, Ti^+, Zr, Zr^+, C;

(b) molecular: H_2, OH, CO, H_2O, CaH, CaO, MgH, MgO, TiO, ZrO.

I found that, for these purposes, sufficient accuracy was obtained without complicated iterative procedures. The elemental abundances were taken from Goldberg et al. (1960), and the molecular constants from Herzberg (1950).

Calculations were carried out for a number of published model atmospheres for the sunspot umbra. In some cases, it was necessary to calculate physical altitudes from the authors' published values for P_g and T as a function of optical depth. Values for the absorption coefficient for the H^- ion were taken from Chandrasekhar (1946) and Geltman (1965) and used for this purpose. For those cases where calculation of hydrostatic pressure was required (see Table 3), the iterative procedure of Weidemann (1955) was used.

The equation for hydrostatic equilibrium, assuming the opacity is due entirely to H^-, and neglecting ionization of H, becomes

$$\frac{dP_g}{d\tau} = \frac{m_H g(1+4B)}{\alpha P_e} \times \frac{P_H+2P_{H_2}}{P_H} \qquad (6)$$

where

B = number abundance of He nuclei

α = absorption coefficient of H^-

Multiplying each side by $P_g d\tau$ and integrating,

$$P_g(\tau) = \left[2m_H g(1+4B) \int_0^{\tau} \frac{P_g}{\alpha P_e} \times \frac{P_H + 2P_{H_2}}{P_H} \, d\tau \right]^{1/2} \qquad (7)$$

This equation is easily integrated, and converges rapidly. I assumed B = 0.16, for convenient comparison with the atmospheres of Zwaan (1965). It should be noted that Makita (1968) found no dependence of T_{er} on the He abundance, so this is of little importance, except for small corrections to the pressures.

Electron pressures were derived from the tables of Zwaan (1965) and Vardya (1961).

The models tested for T_{er} and f-values are listed, with brief descriptions, in Table 3.

The quantities $\Delta T_{er} = T_{er}(\text{observed}) - T_{er}(\text{calculated})$ for TiO and MgH and the f-values for TiO, MgH, and CaH A are the easiest quantities to consider when evaluating these various models. They are listed in Table 4.

Table 3

Model Name	Description
1. Zwaan, 0.48, hyd.	A hydrostatic model based on a solar model with the temperature reduced by adding 0.48 to θ at each point. (Zwaan, 1965)
2. Zwaan, 0.48, sub-hyd.	Like 1., but with pressures reduced by a factor of 4.
3. Zwaan, 0.35, hyd.	Like 1., with $\Delta\theta = 0.35$.
4. Zwaan, 0.35, sub-hyd.	Like 3., but with pressures reduced by a factor of 4.
5. Van't Veer, 1966	A model with sub-hydrostatic pressures, derived from wings of Na and Mg resonance lines. (Van't Veer, 1966)
6. Makita, 1963	A "2-component" model based on photoelectric photometry and atomic spectra. (Makita, 1963)
7. Fricke and Elsässer	A model with sub-hydrostatic pressures, extended here to log $\tau = -4$ by the author. (Fricke and Elsässer, 1965)
8. Henoux, 1968	A model based on the θ-τ relation from infrared continuum photometry of Henoux, with hydrostatic pressures calculated by the author. (Henoux, 1968)
9. Webber, 1969	A new model, based on molecular spectra at small optical depths, calculated in this investigation.

Table 4

Model Name	ΔT_{er}		f-values		
	TiO	MgH	TiO	MgH	CaH A
1. Zwaan, 0.48, hyd.	110	330	3.6×10^{-3}	1.7×10^{-4}	6.8×10^{-3}
2. Zwaan, 0.48, sub-hyd.	180	220	2.7×10^{-3}	1.2×10^{-4}	1.3×10^{-2}
3. Zwaan, 0.35, hyd.	-130	120	3.0×10^{-2}	4.8×10^{-4}	5.0×10^{-2}
4. Zwaan, 0.35, sub-hyd.	-100	190	8.4×10^{-2}	1.2×10^{-3}	0.24
5. Van't Veer, 1966	550	-120	6.0×10^{-3}	1.7×10^{-4}	3.3×10^{-2}
6. Makita, 1963	-630	-270	0.45	9.4×10^{-4}	0.13
7. Fricke and Elsässer	200	270	9.0×10^{-3}	4.3×10^{-4}	2.8×10^{-2}
8. Henoux, 1968	-100	170	4.5×10^{-2}	6.9×10^{-4}	0.11
9. Webber, 1969	0	0	0.28	2.9×10^{-3}	0.64

The value of T_{er} = 3450 ± 300° K adopted for the CaH A bands is just sufficiently questionable to warrant ignoring it in this table. In all the models tested, the rotational temperature for CaH was found to be intermediate between that of TiO and that of MgH (see Figure 2). Since (as will be shown) the measured temperatures of TiO and MgH are probably slightly high, the number of 3450 for CaH is probably close to the correct value, purely by chance.

The contribution functions (integrand of Equation (2)) for the three molecules considered here are shown in Figure 2 for the principal model of Zwaan (1965), along with the contribution functions for weak Fe I lines with excitation potentials of 0.0 and 4.5 eV calculated by Zwaan. This model was chosen for Figure 2 because it is generally representative of the depths of formation of the atomic and molecular lines, and the atomic functions had already been calculated. In each case, the contribution functions have been normalized to a maximum of 1.0 for easy comparison.

In a cool model such as this one, the cut-off of the contribution function for large optical depth is due primarily to the weight function for CaH and

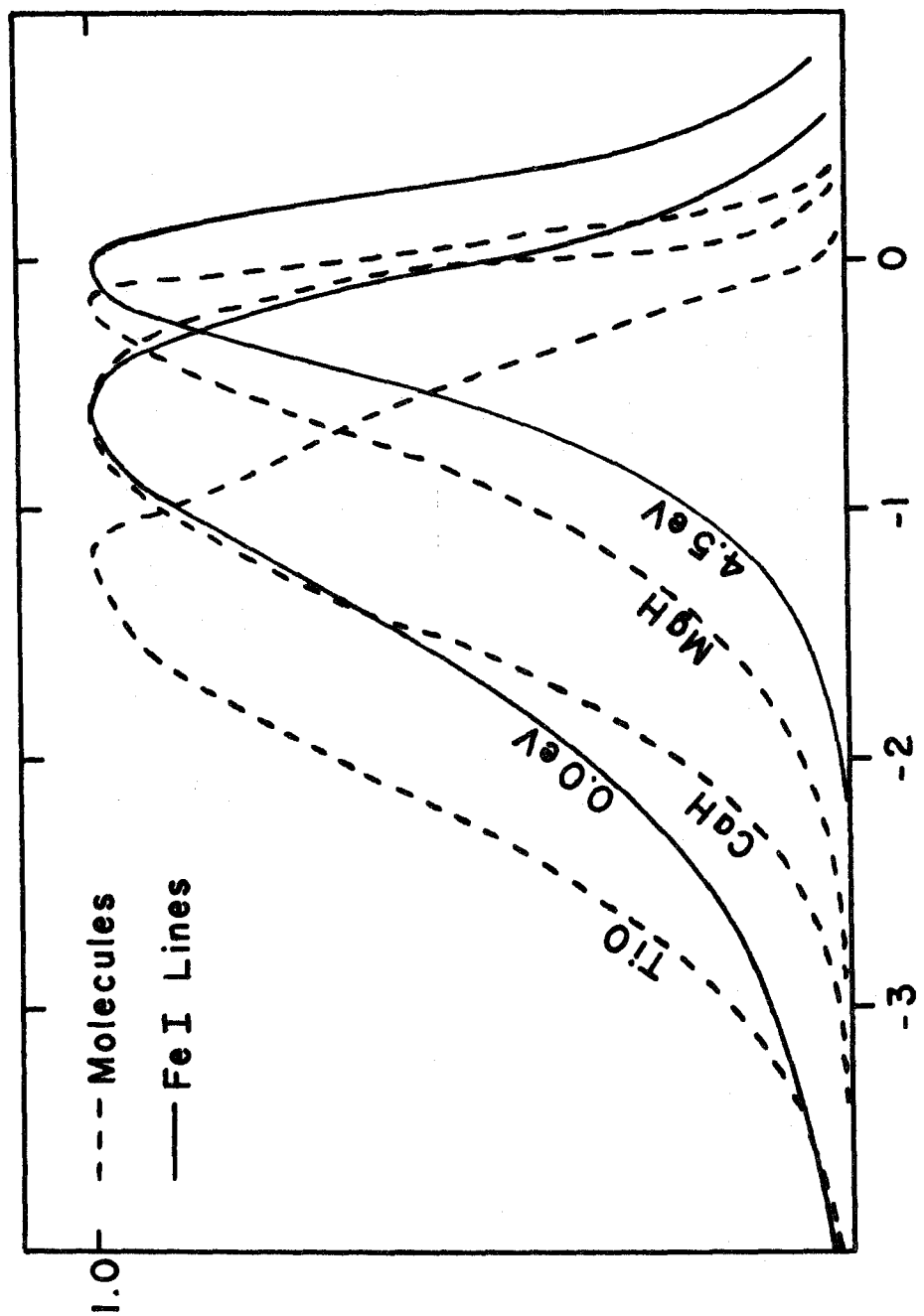

Figure 2. Normalized contribution functions for TiO, CaH, MgH, and weak FeI lines of excitation potential 0.0 and 4.5 eV. The functions for the molecules apply to to the lines of highest measurable J-value in each case.

MgH; there are significant amounts of those two molecules present at higher temperatures, but they contribute little to the observed spectrum. The effect will be even more pronounced for those molecules which are most stable at higher temperatures, such as CO.

The cut-off in the contribution for small optical depth is due primarily to the drop in density of the atmosphere as a whole, although the change in molecular equilibrium with temperature is also important. For these reasons, it is to be expected that the contribution functions for the high-temperature molecules will be quite similar. Therefore, the rotational temperatures obtained from such molecules will be nearly the same, clustering about a maximum value.

I must conclude, then, that the spectra of high-temperature molecules in sunspots will yield little additional information, although it will be of course satisfying to see the prediction verified. The real contribution molecules can make is to the understanding of the outermost layers, where the rotational temperature of TiO in particular does not depend on the cut-off due to the weight function to any significant degree.

V. CONSTRUCTION OF A MODEL

In attempting to contruct a new model using the molecular observations made here, three principal criteria were employed. First, it was required that the effective rotational temperatures obtained from the final model for TiO and MgH agree with the observations exactly. Secondly, according to Zwaan (1965), the observed strengths of the atomic lines cannot be adequately accounted for by a model which is substantially hotter than Zwaan's hydrostatic model with $\Delta\theta = 0.48$, through the region $0.1 \leq \tau \leq 1$. This requirement is reasonable and justifiable. Thirdly, for $\tau > 1$ the model must not be substantially hotter than the temperature distribution found by Henoux (1968). Henoux's results are derived from photoelectric measurements of the infra-red continuum, and are thus much less subject to contamination from photospheric scattered light than other types of data.

A beginning was made by extending the θ-τ relation of Henoux to an optical depth of 0.0001 in a smooth fashion. New θ-τ relations were derived from the original by a parametric expression of the arbitrary form

$$\theta'(\tau) = \theta(\tau)\left[a + b \log \tau + c(\log \tau)^2\right] + d \qquad (8)$$

and the parameters a,b,c,d were adjusted in an attempt to satisfy the criteria listed above. Pressure distributions were assumed to be hydrostatic and were calculated as described in Section IV.

It was found to be impossible to construct a model satisfying all these criteria. A model which predicts exactly the observed T_{er} for TiO and MgH is listed in Table 5. This model is several hundred degrees hotter for $\tau > 0.01$ than the previously mentioned criteria for the atomic and infra-red data would allow. Furthermore, the f-values found for TiO and CaH from this model are unreasonably large.

The objection about f-values may be easily removed by assuming pressures which are sufficiently sub-hydrostatic. However, the predicted T_{er} depends almost entirely on the θ-τ relation, and is virtually uncoupled from any assumptions about the pressure.

There are then two possibilities to account for these discrepancies. Either the atomic and continuum conclusions are incorrect, or the T_{er} found from these observations are all too high. The first possibility is beyond the scope of this paper; the second will be discussed briefly.

In the first place, the difficulties in measuring the molecular lines have already been noted. The scatter of points is large, as seen on the graphs. The lines drawn represent the slopes of the adopted envelopes. A slope implying a temperature 300° K less than the adopted one in each case would not be entirely unreasonable, although the good agreement between the TiO measures for the two separate dates is difficult to understand if such is the case.

It should be noted in passing that Wilson's (1968) tentative model agrees with my θ-τ relation near $\tau = 0.1$, and is in good agreement with the effective temperature (i.e., T at $\tau = 2/3$) of Chitre and Shaviv (1967). However, his temperature gradient is too small to account for the 450° K difference between the T_{er} for TiO and MgH observed here, and thus cannot be quoted as supporting evidence.

I must conclude that the T_{er} obtained from photographic spectra in this manner are probably not reliable enough for definite conclusions to be drawn. Nevertheless, the potential utility of these molecules for probing the outer layers of the sunspot atmosphere cannot be doubted. Greater accuracy in measuring equivalent widths is essential, as is increased laboratory data.

VI. OBSERVATIONAL PROGRAM SUGGESTIONS

The hundreds of lines measured in this investigation represent only a small fraction of the molecular features in sunspots in these regions of the spectrum. It is therefore clear that a comprehensive attempt should be made to identify and measure these features. An extension of the present theoretical calculations should be made, taking into account every single element and all reasonable diatomic and triatomic molecules for which good estimates of the equilibrium constants can be made. A compilation of all laboratory measurements for molecular lines should be made, arranged in order of wavelength.

A second subject needing investigation is whether or not the structure of the umbral atmosphere varies with size, shape, or history of the spot. This is very difficult to determine by means of even the best photoelectric photometry for absolute fluxes, or by atomic spectroscopy, because of contamination by scattered light from the disk. However, T_{er} from the molecular spectra is independent of the total amount of scattered light, and so can be determined with reasonable accuracy regardless of spot size.

It should be noted in this connection that it is unnecessary to measure each time the large number of

lines measured here. This investigation has established which lines of TiO and CaH are particularly useful, in that they are practically free from unknown blends or continuum uncertainty.

A third subject is the variation of T_{er} and absolute line strength with position on the disk. Ideally, one should obtain first-class spectra with a minimum of scattered light for a single, stable spot as it crosses the disk. In practice, this is probably impossible; but if it is established first that the variation in T_{er} between different spots is negligible or predictable, such an investigation would become possible.

Finally, as previously noted, photographic spectra are probably of insufficient accuracy to permit conclusions of greater reliability than those presented here. Photoelectric spectra with carefully calibrated equipment are urgently needed.

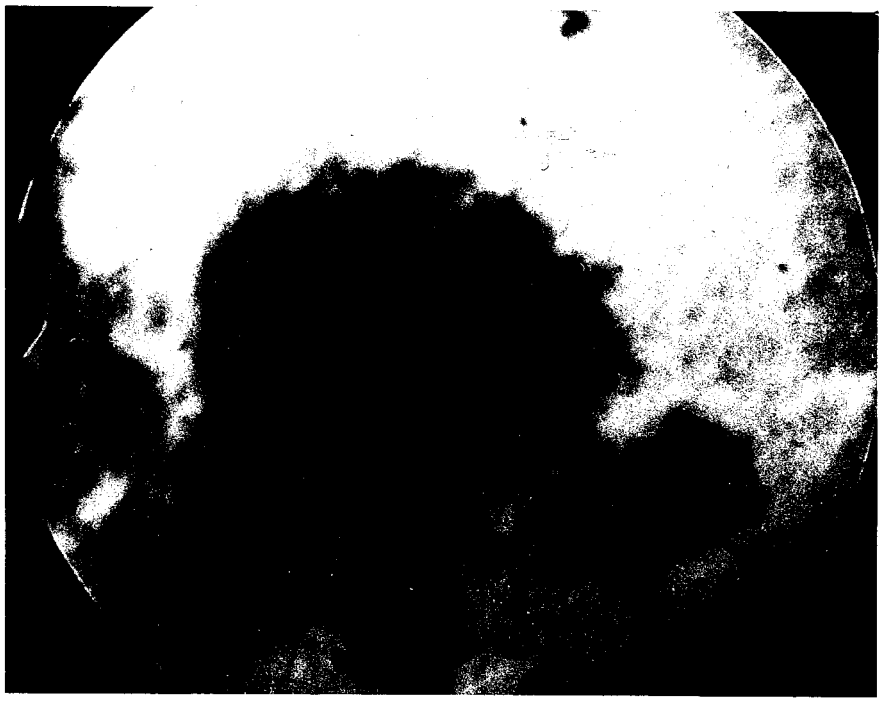

(a)

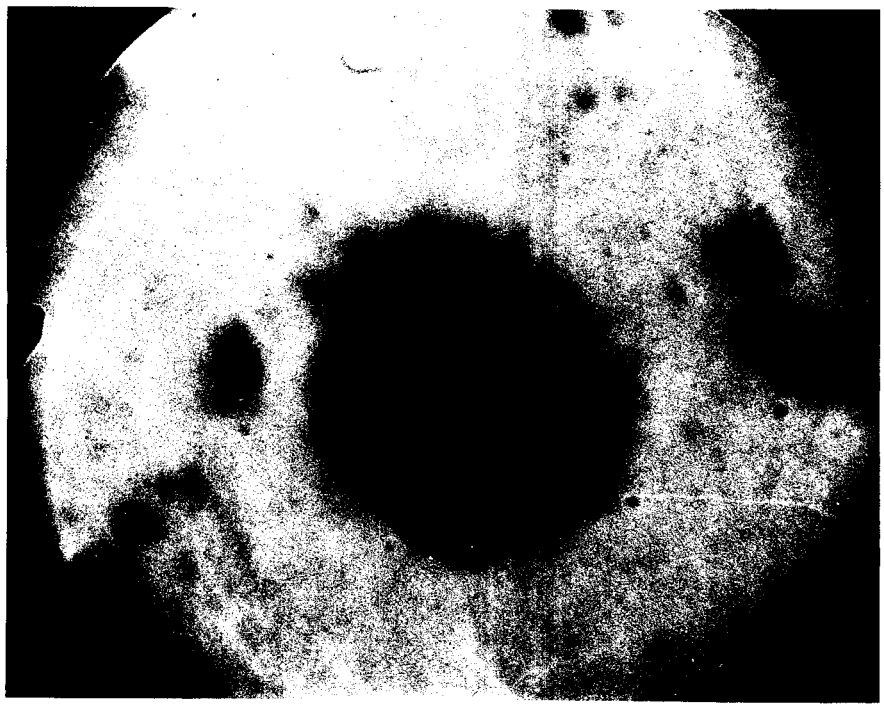

(b)

Figure 3. (a) shows the spot of 10/28/68 at 14:55 U.T. (b) shows the spot of 1/7/69 at 16:42 U.T. See text for comments on the quality of the photographs.

Table 5

τ_{5000}	θ	Log P_g	Log P_e	z(km)
.0001	1.646	3.21	-2.15	0
.0002	1.614	3.36	-1.97	42
.0004	1.577	3.52	-1.78	85
.0007	1.547	3.65	-1.62	122
.001	1.529	3.73	-1.53	144
.002	1.490	3.89	-1.33	191
.004	1.448	4.05	-1.12	238
.007	1.415	4.18	-.95	277
.01	1.389	4.26	-.83	302
.02	1.348	4.41	-.62	352
.04	1.298	4.56	-.39	403
.07	1.252	4.68	-.19	446
.1	1.223	4.76	-.06	473
.2	1.154	4.90	.22	529
.4	1.080	5.04	.50	588
.7	1.022	5.15	.72	640
1.	.963	5.22	.93	674
2.	.860	5.33	1.40	734
4.	.764	5.39	2.04	777
7.	.710	5.43	2.45	807
10.	.683	5.46	2.66	826

Table 6

Wavelength measurements: TiO lines

Identification	λ(lab)	λ(meas)	Quality
$R_2(70)$	5211.77	5211.76	3
$R_3(69)$	12.14	12.13	2
$P_3(48)$	12.41	12.41	2
$P_1(50)$	12.79	12.79	2
$R_1(71)$	12.88	12.87	2
$R_3(70)$	13.63	13.63	2
$P_3(49)$	13.88	13.89	2
$P_1(51)$	14.30	14.30	3
$R_1(72)$	14.42	14.41	2
$R_2(72)$	14.86	14.85	2
$P_3(50)$	15.40	15.39	2
$P_1(52)$	15.86	15.84	2
$R_1(73)$	15.99	15.98	2
$R_3(72)$	16.73	16.71	1
$P_3(51)$	16.94	16.95	3
$R_1(74)$	17.59	17.59	2
$P_2(53)$	17.76	17.76	2
$R_2(74)$	18.08	18.08	1
$R_3(73)$	18.30	18.32	1
$P_3(52)$	18.50	18.51	3
$P_1(54)$	19.03	19.03	2
$R_1(75)$	19.21	19.21	3

Table 6 (cont.)

Wavelength measurements: TiO lines

Identification	λ(lab)	λ(meas)	Quality
$P_2(54)$	5219.38	5219.37	2
$R_3(74)$	19.91	19.90	2
$P_1(55)$	20.66	20.63	3
$R_2(76)$	21.39	21.36	2
$R_3(75)$	21.56	21.53	3
$P_1(56)$	22.27	22.26	2
$R_1(77)$	22.55	22.52	2
$R_2(77)$	23.10	23.08	1
$P_1(57)$	23.98	23.99	2
$P_1(58)$	25.67	25.67	1
$R_1(79)$	25.99	26.00	2
$P_2(58)$	26.11	26.12	2
$P_1(59)$	27.40	27.41	1
$P_2(59)$	27.87	27.87	2
$P_1(60)$	29.16	29.17	3
$R_1(81)$	29.55	29.55	2
$P_2(60)$	29.65	29.65	2
$P_2(61)$	31.46	31.47	2
$R_1(83)$	33.22	33.21	1
$P_2(62)$	33.29	33.29	2
$P_3(61)$	33.74	33.75	2
$P_3(62)$	33.57	33.57	1

Table 6 (cont.)

Wavelength measurements: TiO lines

Identification	λ(lab)	λ(meas)	Quality
$R_3(83)$	5235.68	5235.68	2
$R_2(84)$	35.78	35.79	2
$P_1(64)$	36.43	36.45	2
$P_3(63)$	37.42	37.42	1
$R_3(84)$	37.56	37.57	2
$R_2(85)$	37.70	37.71	3
$P_1(65)$	38.34	38.34	2
$P_3(64)$	39.30	39.30	2
$R_3(85)$	39.48	39.48	2
$R_2(86)$	39.65	39.65	2
$P_1(66)$	40.26	40.25	2
$P_3(65)$	41.20	41.21	3
$R_3(86)$	41.42	41.44	2
$R_2(87)$	41.64	41.64	1
$P_1(67)$	42.21	42.20	2
$R_2(88)$	43.65	43.65	1
$P_1(68)$	44.16	44.17	2
$P_3(67)$	45.11	45.11	3
$R_3(88)$	45.37	45.34	2
$P_2(69)$	46.87	46.86	2
$R_1(90)$	46.94	46.94	1
$R_3(89)$	47.45	47.45	1

Table 6 (cont.)

Wavelength measurements: TiO lines

Identification	λ(lab)	λ(meas)	Quality
$R_2(90)$	5247.75	5247.74	1
$P_1(70)$	48.22	48.19	3
$P_2(70)$	48.92	48.92	2
$R_1(91)$	49.03	49.02	1
$R_3(90)$	49.51	49.51	1
$R_2(91)$	49.84	49.84	2
$P_2(71)$	50.96	50.99	2
$R_3(91)$	51.61	51.59	2
$P_1(72)$	52.33	52.32	3
$P_2(72)$	53.11	53.09	1
$R_3(92)$	53.70	53.72	2
$R_2(93)$	54.15	54.12	2
$P_1(73)$	54.44	54.44	2
$P_2(73)$	55.24	55.22	1
$R_1(94)$	55.43	55.41	1
$R_3(93)$	55.88	55.87	1
$R_2(94)$	56.31	56.30	2
$P_1(74)$	56.58	56.56	3
$P_2(74)$	57.43	57.37	2
$P_3(73)$	57.43	57.44	2
$R_1(95)$	57.60	57.61	1
$R_3(94)$	58.02	57.99	2

Table 6 (cont.)

Wavelength measurements: TiO lines

Identification	λ(lab)	λ(meas)	Quality
$R_2(95)$	5258.53	5258.50	3
$P_1(75)$	58.74	58.72	3
$R_1(96)$	59.85	59.83	2
$R_3(95)$	60.25	60.27	1
$P_1(76)$	60.94	60.94	2
$R_3(96)$	62.50	62.51	2
$P_1(77)$	63.15	63.16	1
$R_3(98)$	67.08	67.10	2
$P_3(78)$	68.51	68.53	1
$P_3(79)$	70.80	70.82	1
$P_2(80)$	70.93	70.94	2
$R_3(100)$	71.77	71.78	3
$P_1(82)$	74.61	74.59	2
$P_3(81)$	75.47	75.49	2
$R_3(102)$	76.58	76.58	2
$P_1(83)$	77.05	77.06	2
$P_3(82)$	77.87	77.86	2
$P_2(83)$	78.08	78.08	2
$R_1(104)$	78.67	78.70	2
$P_1(84)$	79.46	79.50	2
$R_2(104)$	79.76	79.78	1

Table 6 (cont.)

Wavelength measurements: TiO lines

Identification	λ(lab)	λ(meas)	Quality
$P_2(84)$	5280.52	5280.54	2
$R_3(104)$	81.51	81.53	1
$P_3(84)$	82.71	82.72	2
$P_2(85)$	83.01	83.00	1
$R_2(106)$	84.83	84.83	1
$P_2(86)$	85.49	85.50	3
$P_1(87)$	86.92	86.91	1
$R_2(107)$	87.39	87.39	2
$P_2(87)$	88.02	88.02	2
$R_1(108)$	88.83	88.83	1
$R_3(107)$	89.13	89.13	2
$P_1(88)$	89.44	89.44	2
$R_2(108)$	89.99	89.99	1
$P_3(87)$	90.20	90.20	2
$P_2(88)$	90.57	90.58	1
$P_1(89)$	92.01	92.00	2
$P_3(88)$	92.77	92.75	2
$R_1(110)$	94.09	94.09	1
$R_3(109)$	94.35	94.37	1
$R_1(112)$	99.48	99.48	1
$P_1(92)$	99.88	99.88	1

Table 6 (cont.)

Wavelength measurements: CaH A(0,0) lines

Identification	λ(lab)	λ(meas)	Quality
$R_1(36)$	6764.08	6764.09	1
$R_1(35)$	68.95	68.99	2
$R_1(34)$	73.79	73.81	2
$R_1(32)$	83.44	83.47	2
$R_1(31)$	88.29	88.32	2
$R_2(30)$	92.13	92.13	2
$R_2(29)$	96.67	96.64	2
$R_1(29)$	98.00	98.00	2
$R_2(28)$	6801.15	6801.15	2
$R_1(27)$	07.69	07.71	2
$R_2(26)$	10.13	10.15	1
$R_1(26)$	12.53	12.55	2
$R_2(25)$	14.58	14.59	2
$R_1(25)$	17.37	17.41	2
$R_2(24)$	19.02	19.03	2
$R_1(24)$	22.24	22.24	3
$R_2(23)$	23.45	23.46	2
$R_1(23)$	27.07	27.10	1
$R_2(21)$	32.26	32.22	1
$Q_2(43)$	35.31	35.29	2
$Q_1(42)$	36.17	36.16	2
$R_2(20)$	36.61	36.62	2

Table 6 (cont.)

Wavelength measurements: CaH A(0,0) lines

Identification	λ(lab)	λ(meas)	Quality
$R_1(21)$	6836.83	6836.81	2
$Q_1(41)$	40.18	40.16	2
$R_2(19)$	40.93	40.90	2
$Q_2(41)$	43.05	43.03	2
$R_2(18)$	45.20	45.18	1
$R_1(19)$	46.51	46.52	2
$Q_2(40)$	46.84	46.83	3
$Q_1(39)$	48.04	48.03	1
$R_2(17)$	49.47	49.47	1
$Q_2(39)$	50.59	50.60	2
$R_1(18)$	51.36	51.34	2
$R_2(16)$	53.69	53.69	2
$Q_2(38)$	54.23	54.24	2
$R_1(17)$	56.24	56.27	2
$R_1(16)$	61.11	61.14	3
$Q_1(35)$	63.15	63.16	1
$Q_2(35)$	64.86	64.84	2
$Q_1(34)$	66.65	66.67	3
$R_2(11)$	74.19	74.18	2
$Q_2(31)$	77.91	77.92	1
$R_2(10)$	78.14	78.12	2
$R_1(12)$	80.73	80.77	2

Table 6 (cont.)

Wavelength measurements: CaH A(0,0) lines

Identification	λ(lab)	λ(meas)	Quality
$R_2(7)$	6889.44	6889.36	2
$R_1(10)$	90.68	90.62	2
$R_2(5)$	96.51	96.46	1
$Q_2(24)$	97.41	97.37	2
$Q_1(24)$	98.82	98.79	3
$Q_1(23)$	6901.58	6901.56	2
$Q_2(22)$	02.08	02.02	2
$R_2(3)$	03.01	03.04	2
$Q_2(20)$	06.29	06.32	2
$Q_1(21)$	06.86	06.95	2
$R_1(6)$	11.22	11.19	1
$Q_1(19)$	11.79	11.75	2
$Q_2(14)$	15.87	15.84	2
$Q_1(17)$	16.37	16.36	2
$Q_2(13)$	16.96	16.95	3
$Q_1(15)$	20.57	20.59	2
$Q_1(12)$	26.26	26.23	2
$R_1(3)$	27.54	27.57	2
$Q_1(11)$	28.00	27.98	2
$Q_1(8)$	32.81	32.79	2
$Q_1(6)$	35.65	35.68	2
$Q_1(5)$	37.02	37.08	2

Table 6 (cont.)

Wavelength measurements: CaH A(0,0) lines

Identification	λ(lab)	λ(meas)	Quality
$P_2(5)$	6939.30	6939.31	2
$P_1(5)$	56.08	56.11	1
$P_2(10)$	62.20	62.18	2
$P_2(11)$	66.34	66.29	2
$P_1(9)$	66.76	66.74	2
$P_1(10)$	69.58	69.57	3
$P_2(12)$	70.34	70.29	2
$P_1(11)$	72.45	72.43	2
$P_1(12)$	75.28	75.31	2
$P_2(14)$	77.91	77.94	1
$P_1(13)$	78.13	78.16	2
$P_1(14)$	80.95	80.95	2
$P_1(15)$	83.74	83.75	2
$P_1(17)$	89.23	89.26	2
$P_1(19)$	94.48	94.51	2
$P_1(21)$	99.47	99.49	2

Table 6 (cont.)

Wavelength measurements: CaH A(1,1) lines

Identification	λ(lab)	λ(meas)	Quality
$R_1(32)$	6773.25	6773.25	2
$R_2(31)$	77.26	77.28	2
$R_2(30)$	81.52	81.51	2
$R_1(30)$	82.43	82.45	3
$R_2(29)$	85.78	85.82	2
$R_1(29)$	87.06	87.11	2
$R_2(28)$	90.05	90.07	2
$R_1(28)$	91.69	91.72	2
$R_1(27)$	96.35	96.34	2
$R_1(26)$	6800.98	6800.99	1
$R_2(23)$	11.20	11.21	1
$R_2(22)$	15.39	15.39	1
$R_1(21)$	24.18	24.23	2
$R_1(20)$	28.85	28.86	3
$R_1(19)$	33.54	33.53	2
$R_2(17)$	35.98	35.96	2
$R_1(18)$	38.18	38.19	3
$R_1(16)$	47.48	47.50	2
$R_1(15)$	52.14	52.18	2
$Q_2(34)$	60.61	60.63	2
$R_2(10)$	63.06	63.07	2
$Q_1(32)$	63.25	63.29	2

Table 6 (cont.)

Wavelength measurements: CaH A(1,1) lines

Identification	λ(lab)	λ(meas)	Quality
$Q_2(33)$	6863.58	6863.58	2
$R_2(6)$	77.28	77.29	2
$Q_1(27)$	78.31	78.30	2
$Q_2(24)$	86.29	86.26	2
$Q_1(24)$	86.36	86.41	2
$Q_2(23)$	88.33	88.31	2
$Q_1(22)$	91.45	91.42	1
$Q_2(21)$	92.05	91.96	2
$Q_2(17)$	97.98	98.00	2
$Q_2(16)$	99.21	99.18	3
$Q_1(18)$	6900.45	6900.44	2
$Q_2(13)$	01.78	01.74	2
$Q_2(12)$	02.28	02.24	2
$R_1(4)$	05.66	05.73	2
$Q_1(15)$	06.40	06.46	2
$Q_1(9)$	16.17	16.17	2
$Q_1(5)$	21.60	21.65	1
$Q_1(4)$	22.90	22.93	1
$P_1(5)$	38.71	38.70	2
$P_2(10)$	44.70	44.70	2
$P_2(11)$	48.85	48.82	2
$P_1(10)$	52.18	52.20	2

Table 6 (cont.)

Wavelength measurements: CaH A(1,1) lines

Identification	λ(lab)	λ(meas)	Quality
$P_1(11)$	6955.05	6955.07	3
$P_2(14)$	60.44	60.42	2
$P_1(13)$	60.84	60.85	2
$P_1(14)$	63.69	63.70	1
$P_1(15)$	66.52	66.50	2
$P_2(16)$	67.57	67.54	3
$P_1(16)$	69.29	69.26	2
$P_1(18)$	74.65	74.67	2
$P_1(19)$	77.23	77.26	2
$P_2(20)$	80.46	80.43	2
$P_1(21)$	82.17	82.18	2
$P_2(21)$	83.41	83.39	2
$P_1(22)$	84.54	84.53	2
$P_2(22)$	86.22	86.21	1
$P_1(23)$	86.84	86.82	1
$P_2(24)$	91.53	91.59	2
$P_1(26)$	93.10	93.12	3
$P_2(26)$	96.43	96.43	2
$P_1(28)$	96.76	96.80	1
$P_1(29)$	98.49	98.50	2
$P_1(30)$	7000.05	7000.09	1

Table 6 (cont.)

Wavelength measurements: CaH B(0,0) lines

Identification	λ(lab)	λ(meas)	Quality
$R_2(21)$	6237.10	6237.09	2
$R_1(23)$	38.03	38.03	2
$R_1(22)$	43.52	43.50	3
$R_2(19)$	48.47	48.47	2
$R_1(21)$	48.96	48.98	1
$R_1(19)$	59.80	59.80	2
$R_1(17)$	70.43	70.44	2
$R_2(15)$	70.71	70.70	2
$R_1(16)$	75.69	75.67	2
$R_2(14)$	76.13	76.12	2
$R_1(15)$	80.82	80.84	1
$R_2(13)$	81.49	81.47	3
$R_1(14)$	85.93	85.94	2
$R_2(12)$	86.76	86.76	2
$R_2(11)$	91.95	91.95	2
$R_2(10)$	97.06	97.06	3
$R_1(11)$	6300.72	6300.75	1
$R_2(8)$	06.98	06.96	2
$R_1(9)$	10.14	10.15	2
$R_2(7)$	11.78	11.77	2
$R_2(6)$	16.48	16.46	2
$R_2(5)$	21.07	21.06	1

Table 6 (cont.)

Wavelength measurements: CaH B(0,0) lines

Identification	λ(lab)	λ(meas)	Quality
$R_2(4)$	6325.53	6325.52	1
$R_1(4)$	31.57	31.58	1
$P_1(4)$	56.15	56.16	2
$P_2(4)$	57.90	57.85	1
$P_1(5)$	59.28	59.27	1
$P_2(5)$	60.46	60.43	2
$P_1(6)$	62.20	62.21	2
$P_1(7)$	64.94	64.95	2
$P_2(7)$	65.14	65.11	2
$P_2(8)$	67.26	67.23	3
$P_1(8)$	67.53	67.53	3
$P_2(9)$	69.22	69.20	2
$P_1(9)$	69.94	69.96	2
$P_1(10)$	72.20	72.21	1
$P_2(11)$	72.70	72.70	2
$P_2(38)$	73.85	73.86	3
$P_2(12)$	74.23	74.22	2
$P_1(11)$	74.33	74.31	2
$P_2(37)$	74.73	74.72	2
$P_1(12)$	76.24	76.25	2
$P_2(35)$	76.41	76.40	2

Table 6 (cont.)

Wavelength measurements: CaH B(0,0) lines

Identification	λ(lab)	λ(meas)	Quality
$P_2(14)$	6376.84	6376.84	2
$P_2(34)$	77.23	77.22	3
$P_2(31)$	79.38	79.39	2
$P_2(30)$	80.01	80.01	2
$P_2(18)$	80.41	80.44	1
$P_2(29)$	80.56	80.56	2
$P_1(15)$	81.21	81.22	2
$P_1(16)$	82.57	82.59	3
$P_1(41)$	82.79	82.80	2
$P_1(40)$	83.43	83.43	2
$P_1(17)$	83.80	83.81	3
$P_1(18)$	84.89	84.91	3
$P_1(37)$	85.36	85.38	2
$P_1(36)$	85.99	86.01	2
$P_1(35)$	86.57	86.60	2
$P_1(34)$	87.14	87.16	2
$P_1(33)$	87.63	87.66	1
$P_1(22)$	87.99	88.02	1
$P_1(32)$	88.08	88.10	1
$P_1(23)$	88.41	88.39	1
$P_1(31)$	88.47	88.48	1

Table 6 (cont.)

Wavelength measurements: CaH B(1,1) lines

Identification	λ(lab)	λ(meas)	Quality
$R_2(23)$	6238.76	6238.75	2
$R_1(23)$	50.36	50.38	2
$R_1(22)$	55.31	55.32	1
$R_2(19)$	59.45	59.44	2
$R_1(21)$	60.25	60.25	2
$R_2(18)$	64.62	64.60	1
$R_2(17)$	69.79	69.80	2
$R_2(16)$	74.93	74.91	2
$R_1(18)$	75.03	75.04	2
$R_2(15)$	80.05	80.04	1
$R_1(16)$	84.79	84.80	2
$R_2(14)$	85.11	85.07	1
$R_1(15)$	89.61	89.63	1
$R_2(13)$	90.13	90.12	2
$R_1(14)$	94.40	94.41	2
$R_2(12)$	95.09	95.06	1
$R_1(13)$	99.14	99.14	1
$R_2(11)$	99.99	99.97	2
$R_2(10)$	6304.82	6304.80	2
$R_1(11)$	08.43	08.42	2

Table 6 (cont.)

Wavelength measurements: CaH B(1,1) lines

Identification	λ(lab)	λ(meas)	Quality
$R_2(9)$	6309.59	6309.55	3
$R_1(8)$	21.82	21.85	1
$R_1(6)$	30.31	30.34	1
$R_1(4)$	38.29	38.27	1
$R_1(3)$	42.06	42.06	1
$R_1(2)$	45.66	45.66	1
$P_1(2)$	55.74	55.73	1
$P_1(5)$	65.39	65.40	2
$P_2(5)$	66.10	66.06	2
$P_1(6)$	68.28	68.28	1
$P_2(6)$	68.59	68.56	1
$P_2(7)$	70.90	70.87	2
$P_2(8)$	73.04	73.02	2
$P_1(8)$	73.52	73.51	1
$P_2(9)$	75.07	75.06	2
$P_1(9)$	75.90	75.91	2
$P_2(10)$	76.98	76.95	2
$P_1(11)$	80.24	80.25	2
$P_2(12)$	80.41	80.35	1
$P_2(14)$	83.27	83.27	3

Table 6 (cont.)

Wavelength measurements: CaH B(1,1) lines

Identification	λ(lab)	λ(meas)	Quality
$P_2(16)$	6385.73	6385.74	2
$P_2(19)$	88.59	88.59	1
$P_2(20)$	89.33	89.34	2
$P_2(21)$	90.00	90.00	3
$P_1(17)$	90.40	90.44	2
$P_2(22)$	90.56	90.57	2
$P_2(23)$	91.06	91.07	3
$P_2(24)$	91.48	91.48	2
$P_1(18)$	91.73	91.75	1
$P_2(25)$	91.84	91.83	1
$P_2(26)$	92.13	92.14	3
$P_2(27)$	92.37	92.38	2
$P_2(28)$	92.59	92.59	2
$P_2(29)$	92.79	92.78	3
$P_2(31)$	93.14	93.14	2
$P_2(32)$	93.35	93.34	1
$P_2(34)$	93.98	93.98	2
$P_1(20)$	94.06	94.07	2
$P_1(21)$	95.07	95.08	1
$P_1(23)$	96.84	96.84	2

Table 6 (cont.)

Wavelength measurements: CaH B(1,1) lines

Identification	λ(lab)	λ(meas)	Quality
$P_1(24)$	6397.60	6397.60	1
$P_1(25)$	98.29	98.28	2
$P_1(26)$	98.89	98.90	3
$P_1(27)$	99.45	99.46	2
$P_1(30)$	6400.90	6400.89	2
$P_1(31)$	01.32	01.32	2
$P_1(32)$	01.76	01.77	3
$P_1(33)$	02.19	02.19	2
$P_1(34)$	02.72	02.74	2
$P_1(35)$	03.38	03.38	2

Table 7

Good lines in the sunspot spectrum: TiO

Identification	λ(lab)	λ(meas)	Equivalent Width	
			Min	Max
$R_2(70)$	5211.77	5211.76	7.7	12.3
$R_3(69)$	12.14	12.13	(8.6)	(11.3)
$P_3(48)$	12.41	12.41	(9.1)	(11.1)
$P_1(51)$	14.30	14.30	10.2	13.1
$R_1(72)$	14.42	14.41	(9.5)	(12.5)
$P_3(51)$	16.94	16.95	10.1	12.5
$P_3(52)$	18.50	18.51	10.0	13.4
$R_1(75)$	19.21	19.21	6.1	9.9
$P_1(55)$	20.66	20.63	8.0	11.7
$R_3(75)$	21.56	21.53	7.0	12.3
$P_1(60)$	29.16	29.17	10.7	17.5
$R_2(85)$	37.70	37.71	6.7	10.0
$P_3(65)$	41.20	41.21	8.6	12.2
$P_3(67)$	45.11	45.11	7.1	11.0
$P_1(70)$	48.22	48.19	(7.2)	(9.7)
$P_1(72)$	52.33	52.32	7.1	9.8
$P_1(73)$	54.44	54.44	(8.3)	(12.3)

Table 7 (cont.)

Good lines in the sunspot spectrum: TiO

Identification	λ(lab)	λ(meas)	Equivalent Width	
			Min	Max
$P_1(74)$	5256.58	5256.56	8.0	10.3
$R_2(95)$	58.53	58.50	5.3	9.7
$P_1(75)$	58.74	58.72	9.0	12.3
$P_1(76)$	60.94	60.94	(8.1)	
$R_3(100)$	71.77	71.78	3.0	4.6
$P_1(83)$	77.05	77.06	(6.7)	
$P_3(82)$	77.87	77.86	(8.0)	
$P_2(86)$	85.49	85.50	4.8	8.9
$R_3(107)$	89.13	89.13	(2.1)	(5.3)

Table 7 (cont.)

Good lines in the sunspot spectrum: CaH A(0,0)

Identification	λ(lab)	λ(meas)	Equivalent Width	
			Min	Max
$R_1(29)$	6798.00	6798.00	(13.0)	(15.8)
$R_2(25)$	6814.58	6814.59	(14.5)	(19.7)
$R_1(24)$	22.24	22.24	14.8	21.3
$Q_2(40)$	46.84	46.83	12.6	17.9
$Q_2(38)$	54.23	54.24	(11.7)	(16.5)
$R_1(17)$	56.24	56.27	(16.7)	(24.8)
$R_1(16)$	61.11	61.14	13.1	21.4
$Q_1(34)$	66.65	66.67	15.4	25.4
$Q_1(24)$	98.82	98.79	28.0	33.1
$Q_1(19)$	6911.79	6911.75	(17.5)	(31.3)
$Q_2(14)$	15.87	15.84	(21.8)	(29.8)
$Q_2(13)$	16.96	16.95	23.0	28.7
$Q_1(12)$	26.26	26.23	(27.6)	(36.2)
$P_1(10)$	69.58	69.57	19.3	25.0

Table 7 (cont.)

Good lines in the sunspot spectrum: CaH A(1,1)

Identification	λ(lab)	λ(meas)	Equivalent Width	
			Min	Max
$R_1(32)$	6773.25	6773.25	(15.5)	(21.8)
$R_1(30)$	82.43	82.45	12.2	23.1
$R_1(20)$	6828.85	6828.86	13.7	21.2
$R_1(19)$	33.54	33.53	(14.1)	(19.9)
$R_1(18)$	38.18	38.19	14.1	18.9
$Q_2(34)$	60.61	60.63	(16.3)	(17.1)
$Q_2(16)$	99.21	99.18	18.8	31.9
$P_1(11)$	6955.05	6955.07	17.4	26.7
$P_2(14)$	60.44	60.42	(20.9)	(26.0)
$P_2(16)$	67.57	67.54	18.9	27.4
$P_1(16)$	69.29	69.26	(21.1)	(30.7)
$P_1(26)$	93.10	93.12	18.3	22.7

Table 7 (cont.)

Good lines in the sunspot spectrum: CaH B(0,0)

Identification	λ(lab)	λ(meas)	Equivalent Width	
			Min	Max
$R_1(23)$	6238.03	6238.03	(5.7)	(8.6)
$R_1(22)$	43.52	43.50	7.9	14.9
$R_2(19)$	48.47	48.47	(11.5)	(14.5)
$R_2(15)$	70.71	70.70	(8.9)	(15.4)
$R_2(13)$	81.49	81.47	6.7	11.9
$R_2(12)$	86.76	86.76	(6.6)	(13.9)
$R_2(10)$	97.06	97.06	13.5	18.4
$P_1(4)$	6356.15	6356.16	(5.4)	(9.0)
$P_2(7)$	65.14	65.11	(8.7)	(17.0)
$P_2(8)$	67.26	67.23	12.5	
$P_1(8)$	67.53	67.53	9.8	
$P_1(9)$	69.94	69.96	(21.2)	
$P_2(11)$	72.70	72.70	(13.9)	(22.4)
$P_2(38)$	73.85	73.86	12.0	
$P_2(34)$	77.23	77.22	19.6	22.5
$P_2(30)$	80.01	80.01	(10.2)	(15.6)
$P_1(16)$	82.57	82.59	12.5	18.6
$P_1(40)$	83.43	83.43	(12.0)	
$P_1(17)$	83.80	83.81	16.6	
$P_1(18)$	84.89	84.91	16.3	22.0
$P_1(37)$	85.36	85.38	(8.2)	(11.1)

Table 7 (cont.)

Good lines in the sunspot spectrum: CaH B(1,1)

Identification	λ(lab)	λ(meas)	Equivalent Width	
			Min	Max
$R_2(23)$	6238.76	6238.75	(6.1)	(7.8)
$R_1(21)$	60.25	60.25	(6.2)	
$R_1(18)$	75.03	75.04	(8.4)	
$R_2(10)$	6304.82	6304.80	(6.0)	(9.4)
$R_2(9)$	09.59	09.55	6.6	12.4
$P_1(5)$	65.39	65.40	(6.2)	(9.6)
$P_2(8)$	73.04	73.02	(14.2)	(26.1)
$P_2(9)$	75.07	75.06	(11.6)	
$P_2(14)$	83.27	83.27	11.5	
$P_2(21)$	90.00	90.00	10.6	14.0
$P_2(23)$	91.06	91.07	8.8	13.0
$P_2(26)$	92.13	92.14	11.2	15.0
$P_2(29)$	92.79	92.78	13.5	16.0
$P_1(23)$	96.84	96.84	(13.6)	(18.1)
$P_1(26)$	98.89	98.90	12.0	15.8
$P_1(32)$	6401.76	6401.77	17.4	21.5
$P_1(35)$	03.38	03.38	(18.1)	(25.8)

Table 7 (cont.)

Good lines in the sunspot spectrum: MgH

Identification	λ(lab)	λ(meas)	Equivalent Width	
			Min	Max
$Q_2(39)$	5049.18	5049.22	(12.8)	(20.4)
$Q_2(35)$	73.38	73.42	19.4	27.6
$Q_2(29)$	5106.21	5106.25	(18.9)	(27.3)
$R_2(16)$	06.85	06.87	(15.7)	(30.2)
$Q_1(25)$	25.81	25.85	(10.5)	(29.1)
$P_1(33)$	77.76	77.64	(11.9)	(19.5)
$P_2(29)$	90.56	90.55	14.1	20.3
$P_1(28)$	93.86	93.88	15.2	27.5
$P_1(24)$	5202.99	5202.97	14.7	25.5

REFERENCES

Babcock, H.D.: 1945, Ap. J., 102, 154.

Chandrasekhar, S.: 1946, Ap. J., 104, 444.

Chitre, S.M., Shaviv, G.: 1967, Solar Phys., 2, 150.

Christy, A.: 1929, Phys. Rev., 33, 701.

ESSA: 1968, 1969, Solar-Geophysical Data, Nos. 290, 291, 292, 294, 295.

Fricke, K., Elsässer, H.: 1965, Zs. f. Ap., 63, 35.

Geltman, S.: 1965, Ap. J., 141, 376.

Goldberg, L., Muller, E.A., Aller, L.H.: 1960, Ap. J. Suppl., 5, No. 45.

Henoux, J.C.: 1968, Ann. d'Ap., 31, 511.

Herzberg, G.: 1950, Spectra of Diatomic Molecules.

Hitchcock, J.L.: 1965, Publ. Astr. Soc. Pacific, 77, 290.

Hulthen, E.: 1927, Phys. Rev., 29, 97.

Laborde, G.: 1961, Ann. d'Ap., 24, 89.

Lagerquist, A., Uhler, U., Barrow, R.F.: 1954, Ark. Fys., 8, 285.

Liberale, G., Weniger, S.: 1969, Physica, 41, 47.

Makita, M.: 1963, Publ. Astr. Soc. Japan, 15, 145.

Makita, M.: 1968, Solar Phys., 3, 557.

Moore, C.E., Minnaert, M.G.J., Houtgast, J.: 1966, The Solar Spectrum 2935 A to 8770 A.

Mulliken, R.S.: 1931, Rev. Mod. Phys., 3, 89.

Phillips, J.G.: 1969, Ap. J., 157, 449.

Schadee, A.: 1964, B.A.N., 17, 311.

Schadee, A.: 1966, Ap. J., 145, 348.

Tsuji, T.: 1964, Ann. Astr. Obs. Tokyo, Second Series, IX, No. 1.

Vardya, M.S.: 1961, Ap. J., 133, 107.

Veer, F. Van't: 1966, Proceedings of the Meeting on Sunspots, Florence, 1964.

Watson, W.W., Rudnick, P.: 1927, Phys. Rev., 29, 413.

Weidemann, V.: 1955, Zs. f. Ap., 36, 101.

Wilson, P.R.: 1968, Solar Phys., 5, 351.

Zwaan, C.: 1965, Rech. Astr. Obs. Utrecht, 17, Part 4.

APPENDIX

The accompanying figures are plots of $\log(W_J/S_J)$ against $F_v(J)$ for the molecules considered. A filled data point indicates a measurement for which there was no apparent difference between the true and local continuum levels; it does not necessarily imply greater reliability. Solid straight lines show the adopted maximum or minimum envelopes of the points. Dashed straight lines show the envelopes for individual branches which appear to differ sisnificantly from the overall envelopes.

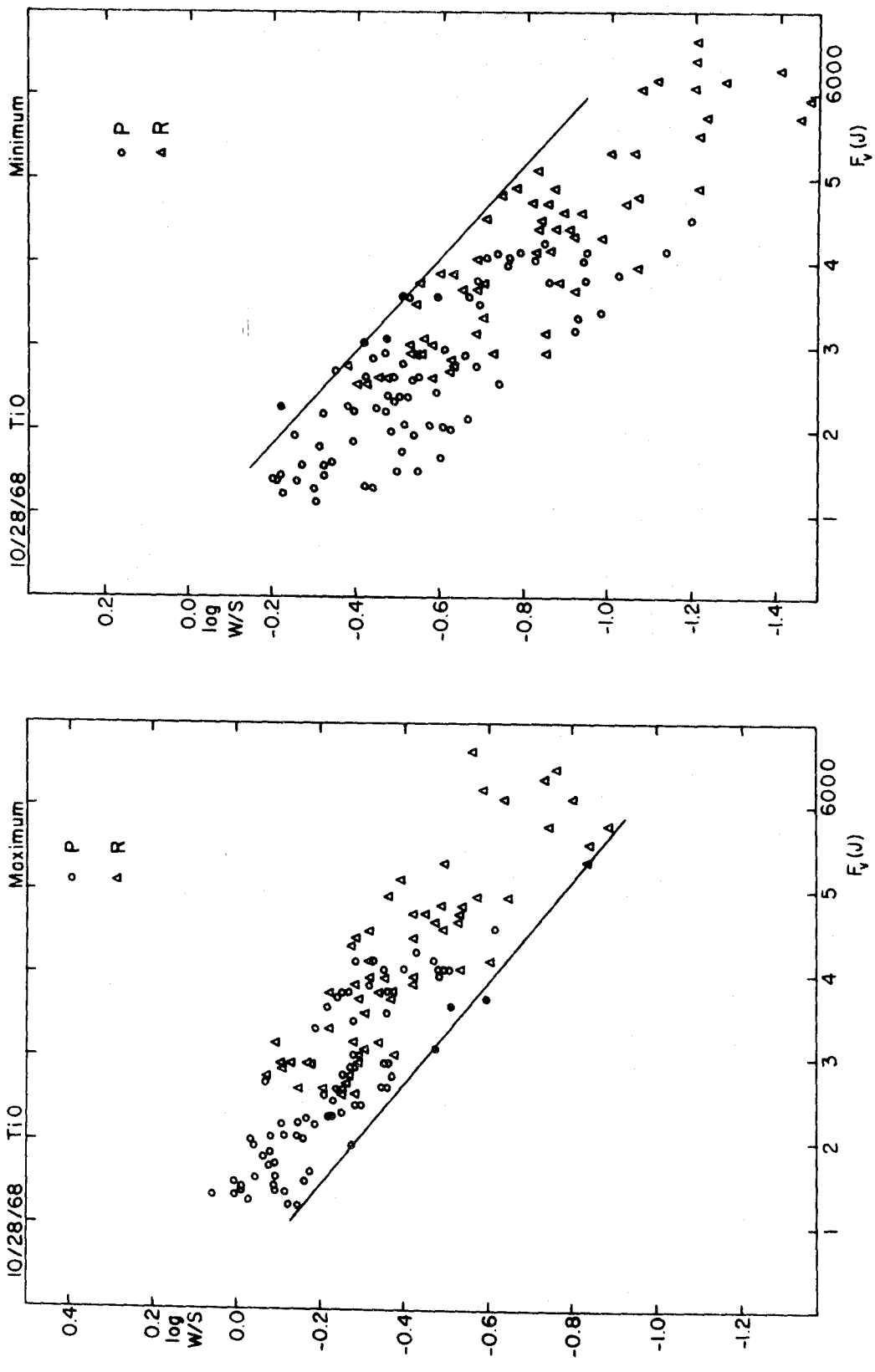
10/28/68 TiO
Minimum
P
R
log W/S
F_v(J)
10/28/68 TiO
Maximum
P
R
log W/S
F_v(J)

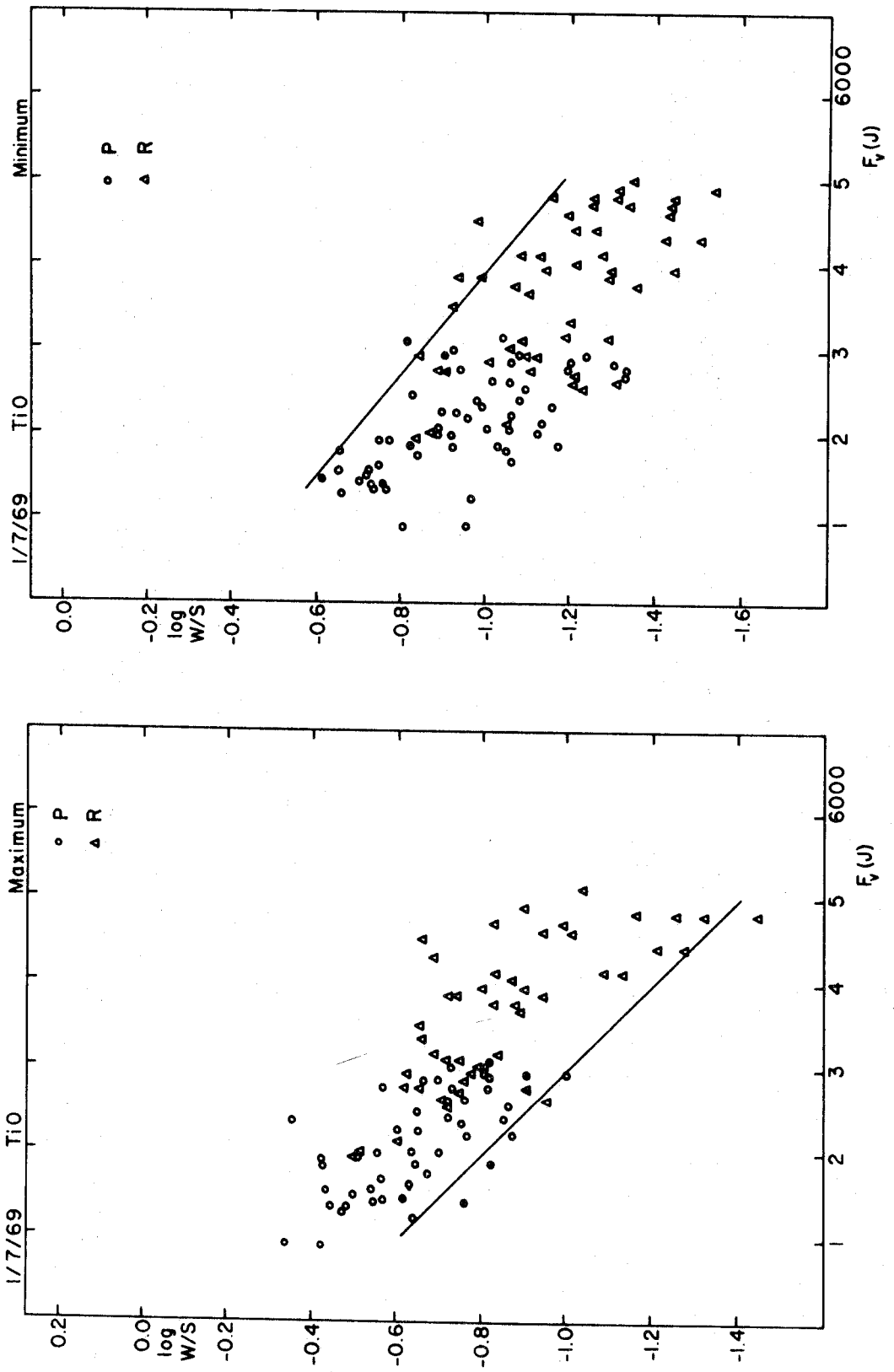
Minimum
TiO
1/7/69
P
R
log W/S
0.0
-0.2
-0.4
-0.6
-0.8
-1.0
-1.2
-1.4
-1.6
1
2
3
4
5
6000
F_v(J)
Maximum
TiO
1/7/69
P
R
log W/S
0.2
0.0
-0.2
-0.4
-0.6
-0.8
-1.0
-1.2
-1.4
1
2
3
4
5
6000
F_v(J)

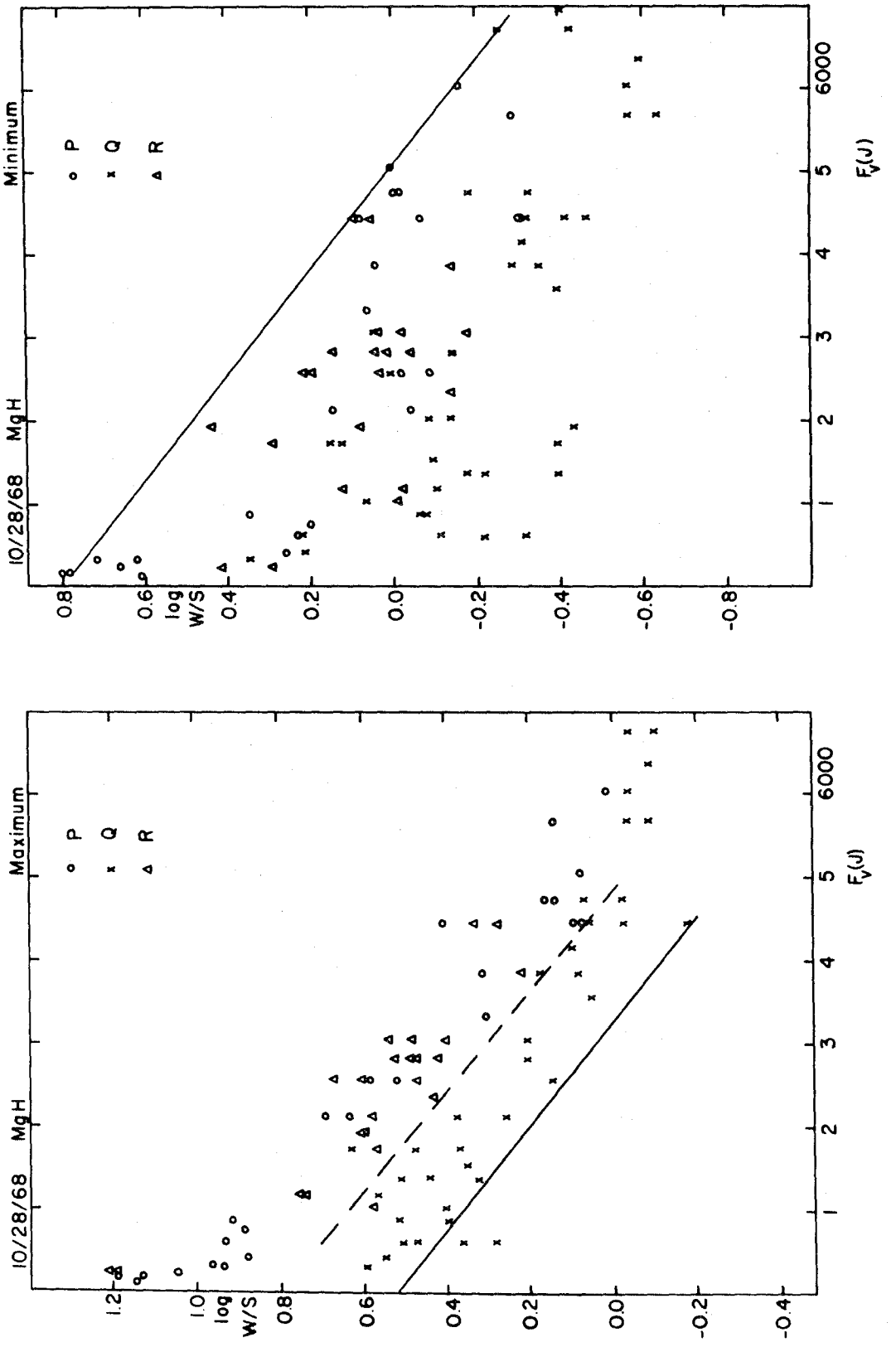
Minimum
10/28/68 MgH
P
Q
R
log W/S
$F_V(J)$
Maximum
10/28/68 MgH
P
Q
R
log W/S
$F_V(J)$

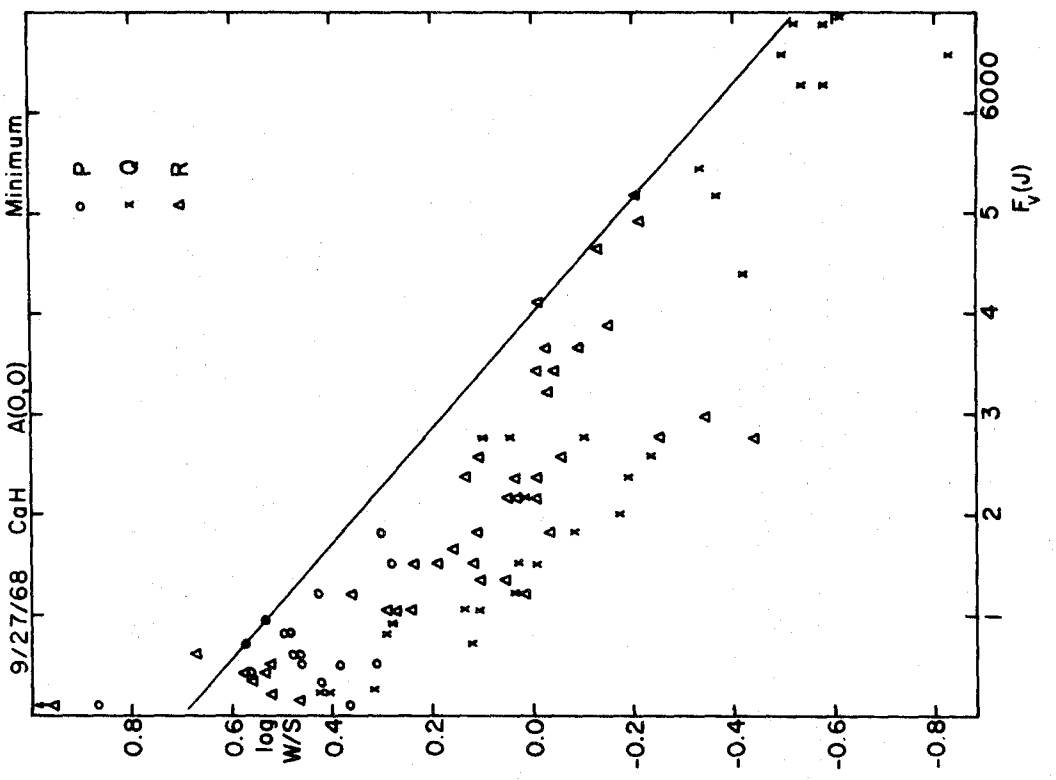
9/27/68 CaH A(0,0) Minimum
P
Q
R
log W/S
$F_v(J)$

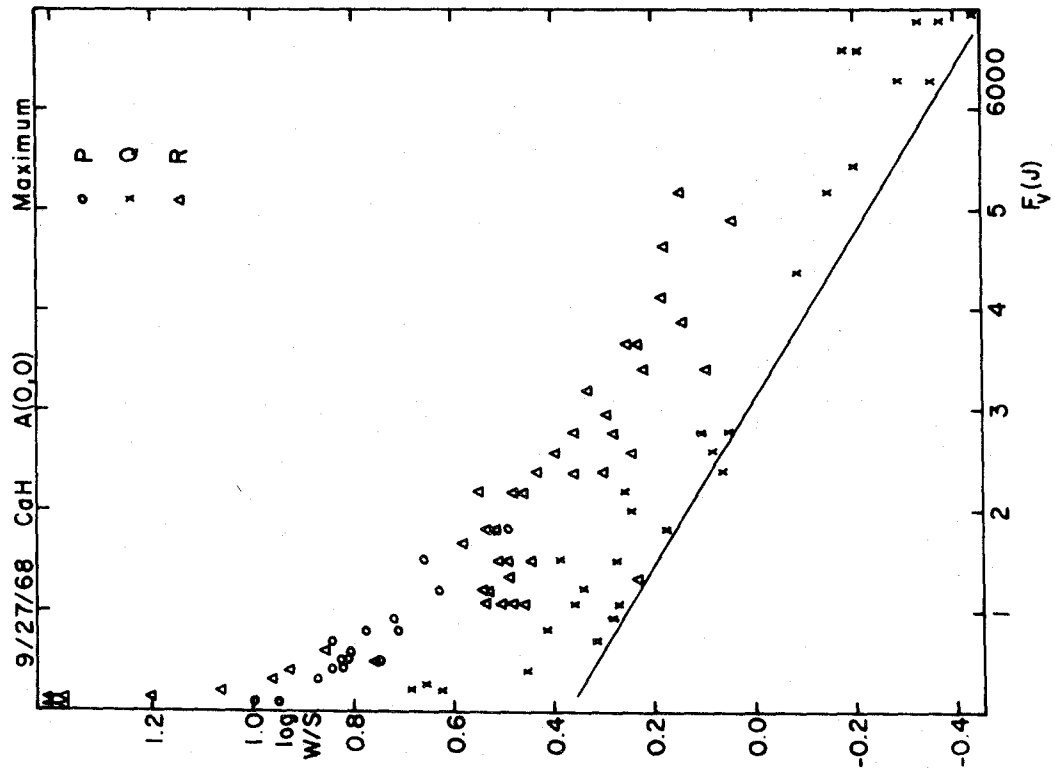
9/27/68 CaH A(0,0) Maximum
P
Q
R
log W/S
$F_v(J)$

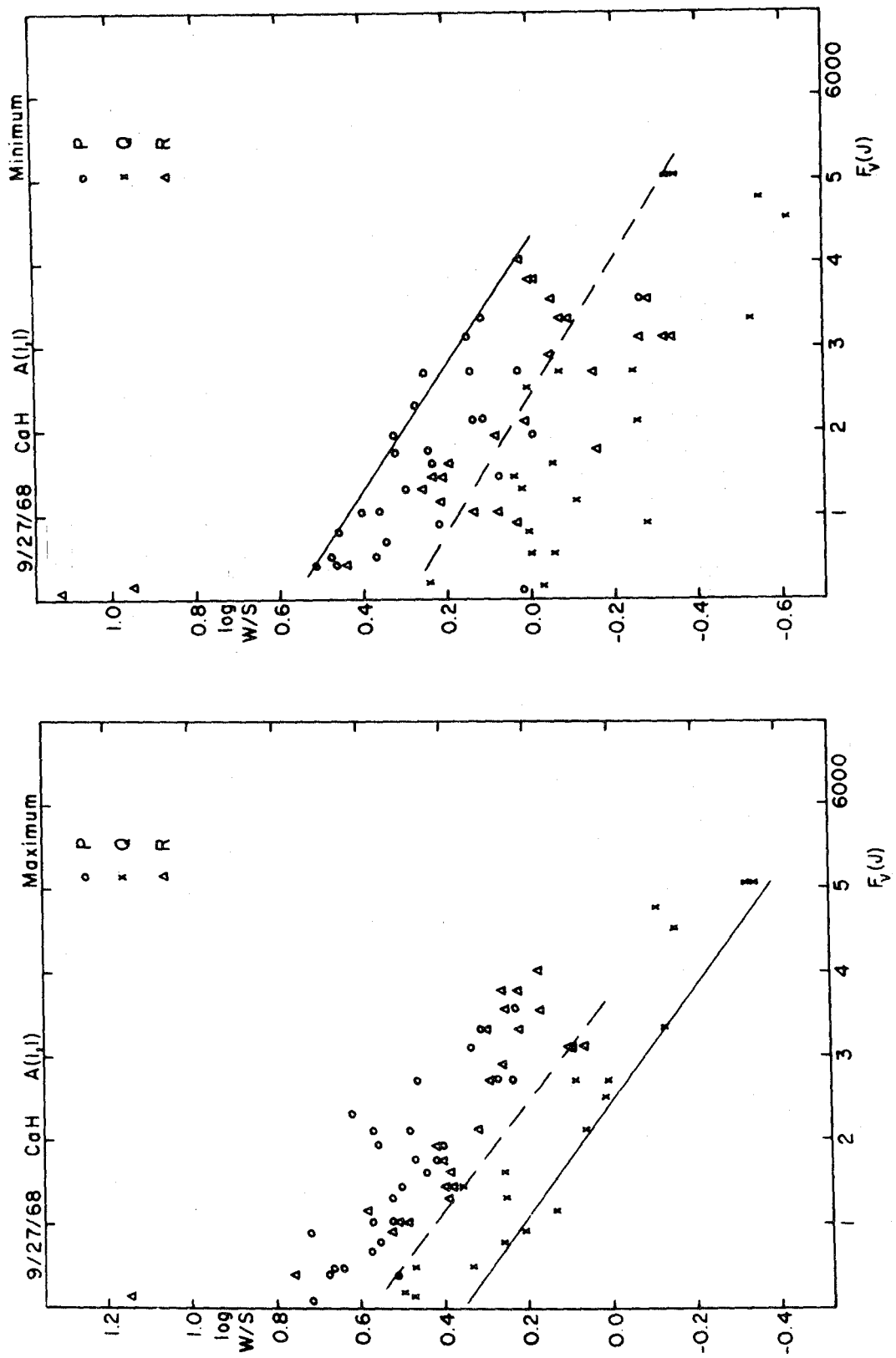
Minimum
9/27/68 CaH A(1,1)
P
Q
R
log W/S
$F_v(J)$
Maximum
9/27/68 CaH A(1,1)
P
Q
R
log W/S
$F_v(J)$

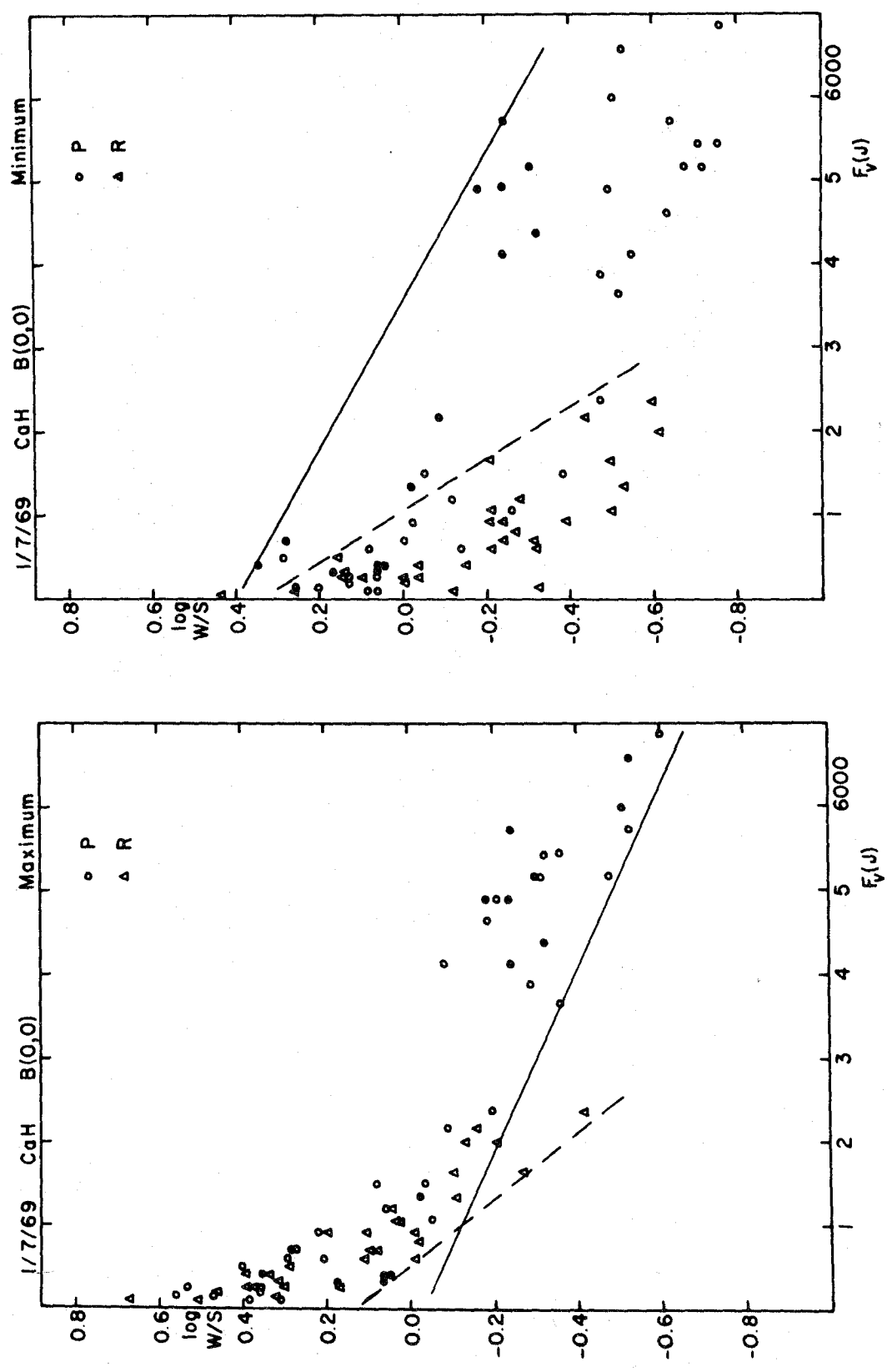
Minimum
1/7/69 CaH B(0,0)
P
R
log W/S
$F_v(J)$
Maximum
1/7/69 CaH B(0,0)
P
R
log W/S
$F_v(J)$

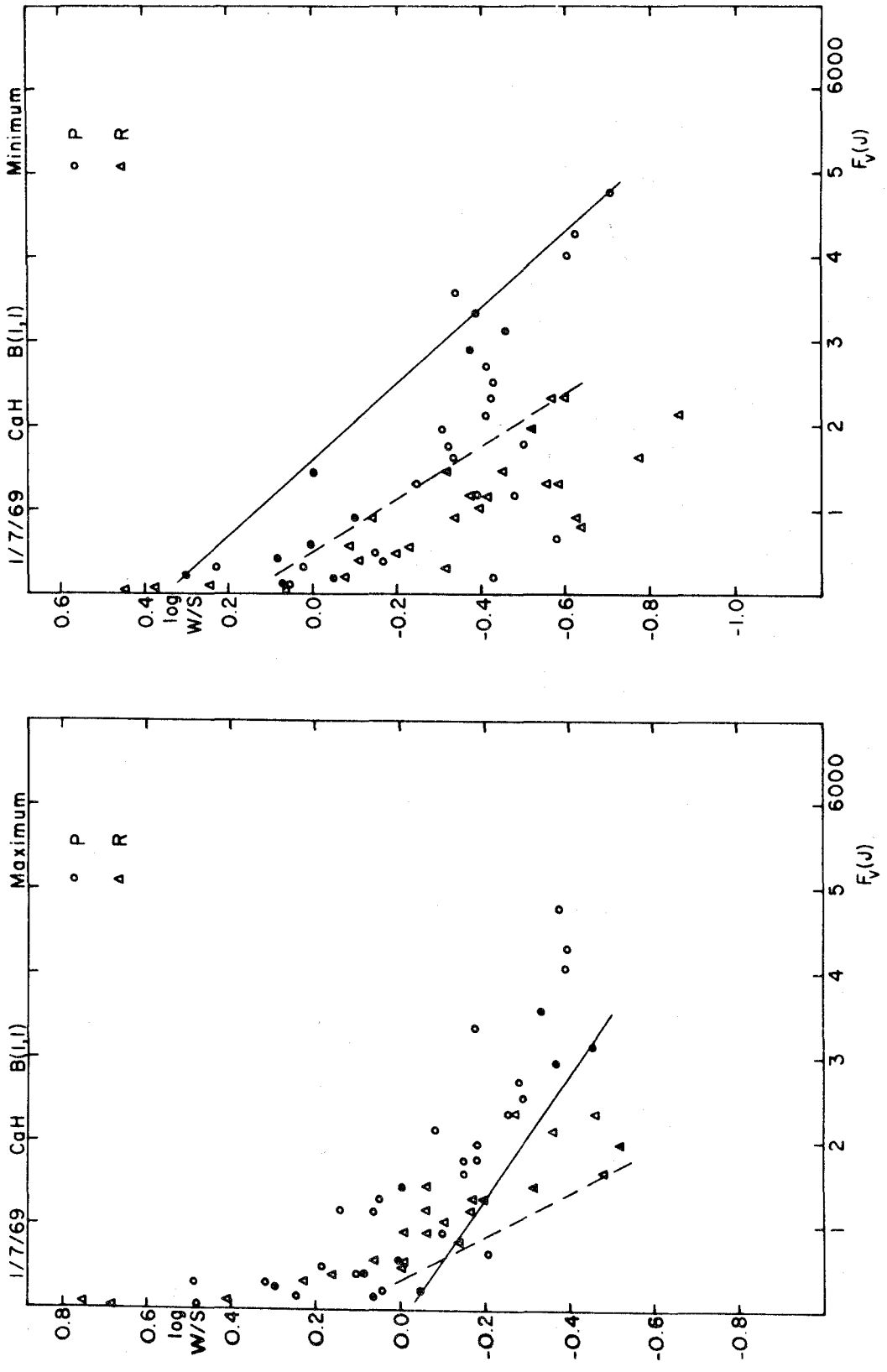
1/7/69 CaH B(1,1) Minimum
P
R
log W/S
$F_v(J)$
1/7/69 CaH B(1,1) Maximum
P
R
log W/S
$F_v(J)$